



1 **Contribution of HONO to the atmospheric oxidation capacity in an industrial zone**
2 **in the Yangtze River Delta region of China**

3 Jun Zheng^{1*}, Xiaowen Shi¹, Yan Ma^{1,2}, Xinrong Ren^{3,4,5}, Halim Jabbour¹, Yiwei Diao^{1,6}, Weiwei Wang⁶, Yifeng
4 Ge¹, Yuchan Zhang¹, and Wenhui Zhu¹

5 ¹Collaborative Innovation Center of Atmospheric Environment and Equipment Technology, Nanjing University
6 of Information Science & Technology, Nanjing 210044, China

7 ²NUIST Reading Academy, Nanjing University of Information Science & Technology, Nanjing 210044, China

8 ³Air Resources Laboratory, National Oceanic and Atmospheric Administration, College Park, Maryland, USA

9 ⁴Department of Atmospheric and Oceanic Science, University of Maryland, College Park, Maryland, USA

10 ⁵Cooperative Institute for Satellite Earth System Studies, University of Maryland, College Park, Maryland, USA

11 ⁶Key Laboratory for Aerosol-Cloud-Precipitation of China Meteorological Administration, Department of
12 Atmospheric Physics, Nanjing University of Information Science and Technology, Nanjing 210044, China

13

14 *Correspondence to: Dr. Jun Zheng (zheng.jun@nuist.edu.cn)*

15 *Address: School of Environmental Science and Engineering, Nanjing University of Information*

16 *Science & Technology, Nanjing 210044, China*

17 *Tel.: +86-18251919852*

18 *Fax: +86-25-58731090*

19



20 **Key points:**

- 21 • High levels of HONO, with an average of 1.32 ± 0.92 ppbv, were observed near one of the largest industrial
22 zone in the YRD region of China.
- 23 • HONO photolysis and alkene ozonolyses contributed the most of OH production and hence the atmospheric
24 oxidation capacity.
- 25 • High HONO concurred with high loading of $PM_{2.5}$, indicating potential synergetic effects.
- 26 • Heterogeneous formation mechanisms were the most important daytime HONO sources and were further
27 enhanced by sunlight.

28 **Abstract**

29 A suite of instruments were deployed to simultaneously measure nitrous acid (HONO), nitrogen oxides (NO_x
30 = $NO + NO_2$), carbon monoxide (CO), ozone (O_3), volatile organic compounds (VOCs, including formaldehyde
31 (HCHO)) and meteorological parameters near a typical industrial zone in Nanjing of the Yangtze River Delta region,
32 China. High levels of HONO were detected using a wet chemistry-based method. HONO ranged from 0.03-7.04
33 ppbv with an average of 1.32 ± 0.92 ppbv. Elevated daytime HONO was frequently observed with a minimum of
34 several hundreds of pptv on average, which cannot be explained by the homogeneous $OH + NO$ reaction (P_{OH+NO})
35 alone, especially during periods with high loadings of particulate matters ($PM_{2.5}$). The HONO chemistry and its
36 impact on atmospheric oxidation capacity in the study area were further investigated using a MCM-box model. The
37 results show that the average hydroxyl radical (OH) production rate was dominated by the photolysis of HONO
38 (7.13×10^6 molecules $cm^{-3} s^{-1}$), followed by ozonolysis of alkenes (3.94×10^6 molecules $cm^{-3} s^{-1}$), photolysis of O_3
39 (2.46×10^6 molecules $cm^{-3} s^{-1}$) and photolysis of HCHO (1.60×10^6 molecules $cm^{-3} s^{-1}$), especially within the plumes
40 originated from the industrial zone. The observed similarity between HONO/ NO_2 and HONO in diurnal profiles
41 strongly suggests that HONO in the study area was likely originated from NO_2 heterogeneous reactions. The



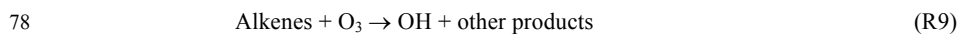
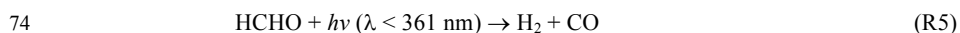
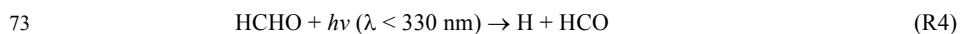
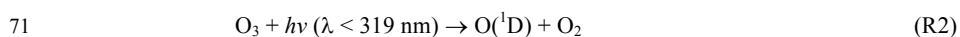
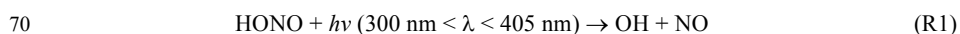
42 average nighttime NO_2 to HONO conversion rate was determined to be $\sim 0.9\% \text{ hr}^{-1}$. Good correlation between
43 nocturnal HONO/ NO_2 and the products of particle surface area density (S/V) and relative humidity (RH), S/V·RH,
44 supports the heterogeneous $\text{NO}_2/\text{H}_2\text{O}$ reaction mechanism. The other HONO source, designated as P_{unknown} , was
45 about twice as much as $P_{\text{OH+NO}}$ on average and displayed a diurnal profile with an evidently photo-enhanced feature,
46 i.e., photosensitized reactions of NO_2 may be an important daytime HONO source. Nevertheless, our results suggest
47 that daytime HONO formation was mostly due to the light-induced conversion of NO_2 on aerosol surfaces but
48 heterogeneous NO_2 reactions on ground surface dominated nocturnal HONO production. Concurrent elevated
49 HONO and $\text{PM}_{2.5}$ levels strongly indicate that high HONO may increase the atmospheric oxidation capacity and
50 further promote the formation of secondary aerosols, which may in turn synergistically boost NO_2/HONO
51 conversion by providing more heterogeneous reaction sites.

52 **1 introduction**

53 Nitrous acid (HONO) plays an important role in tropospheric photochemistry because its fast photolysis
54 contributes to the formation of hydroxyl (OH) radical, which is an essential atmospheric oxidant that initiates the
55 oxidation of volatile organic compounds (VOC) to form organic peroxy radicals (RO_2) and hydroperoxyl radical
56 (HO_2). In the presence of nitrogen oxides ($\text{NO}_x = \text{NO} + \text{NO}_2$), these free radicals are the fundamental driving force
57 of photochemical reaction cycles that lead to the formation of ground-level ozone (O_3) and secondary organic
58 aerosols (SOA) (Finlayson-Pitts and Pitts, 1999; Xue et al., 2016). Besides HONO photolysis (R1), the major
59 known OH radical initiation sources include photolysis of O_3 (R2 and R3) and formaldehyde (HCHO) (R4 to R8),
60 and ozonolysis of alkenes (R9) (Finlayson-Pitts and Pitts, 1999). Nevertheless, many field studies have
61 demonstrated that HONO may strongly affect atmospheric oxidation capacity in various environments (Bernard et
62 al., 2016; Elshorbany et al., 2009; Elshorbany et al., 2010; Zhou et al., 2002). In early studies, HONO was believed
63 to be only important as NO_x reservoir during nighttime, when HONO can accumulate in the atmosphere and give



64 a boost of photochemistry in the following early morning (Platt et al., 1980). However, recent field studies have
65 demonstrated that high concentrations of HONO are often present in the relatively polluted urban areas during the
66 day. Because of high levels of HONO, the photolysis of HONO becomes an important OH source not only in the
67 early morning but also throughout the day and can contribute up to 30-90% of OH radical during daytime (Acker
68 et al., 2006; Hendrick et al., 2014; Kleffmann et al., 2005; Neftel et al., 1996; Spataro et al., 2013; Su et al., 2008;
69 Zhou et al., 2002).



79 Despite the significance of HONO in daytime photochemistry, the sources and formation mechanisms of
80 HONO, especially during daytime, are still uncertain. Traditionally, the reaction between NO and OH was thought
81 to be the most important homogeneous source for HONO (Perner and Platt, 1979):



83 However, reaction R10 alone cannot sustain the high HONO level observed during daytime in many studies, in
84 which the observed HONO levels were often an order of magnitude greater than the modeled HONO with only
85 homogeneous HONO source (R10) included in the model (Ren et al., 2010; Tang et al., 2015). Nevertheless, higher
86 than expected OH observed in several studies (Hofzumahaus et al., 2009) may explain partially observed higher



87 than model predicted HONO levels. It has been suggested that HONO may be emitted directly by incomplete
88 combustion processes, such as vehicle exhaust (Kirchstetter et al., 1996; Kurtenbach et al., 2001; Liang et al., 2017;
89 Nakashima and Kajii, 2017; Trinh et al., 2017; Xu et al., 2015) and biomass burning (Müller et al., 2016; Neuman
90 et al., 2016; Nie et al., 2015; Rondon and Sanhueza, 1989). However, such strong but sporadic point sources could
91 not account for the widely observed daytime HONO in the polluted areas (Elshorbany et al., 2012; Wang et al.,
92 2017). Recently, many other HONO formation pathways have been proposed. Su et al. (2011) pointed out that
93 HONO can be released from soil nitrite, which was formed through biological nitrification and denitrification
94 processes. Recent studies demonstrated that the pH and organic content of soil could influence the HONO emission
95 rate (Scharko et al., 2017; Sörgel et al., 2015). In addition, vertical profiles of HONO measurements indicated that
96 HONO was very likely originated from the ground surface (Kleffmann et al., 2003; VandenBoer et al., 2013; Wong
97 et al., 2011; Wong et al., 2013). However, the presence of in-situ HONO sources in the air masses aloft cannot be
98 ruled out (Wong et al., 2013; Zhang et al., 2009).

99 Several heterogeneous processes have been drawn substantial attention and are proposed as the major HONO
100 sources, including: (1) heterogeneous conversion of NO₂ on wet surface (Finlayson-Pitts et al., 2003), which could
101 be an important nocturnal HONO source; (2) NO₂ heterogeneous reaction with fresh soot particles (Ammann et al.,
102 1998; Gerecke et al., 1998; Han et al., 2017a; Monge et al., 2010) and semi-volatile organic compound emitted
103 from diesel exhausts (George et al., 2005; Gutzwiller et al., 2002), which could be an important process because it
104 is 1 to 2 orders of magnitude faster than the typically proposed heterogeneous reaction of 2NO₂ + H₂O; (3)
105 photosensitized reaction of NO₂ on surfaces of mineral dust (Ndour et al., 2008), humic acid (Han et al., 2017b;
106 Wall and Harris, 2016), and ground surface (i.e., certain reactions such as NO₂ + humic acids on ground surfaces)
107 (Wong et al., 2012), which has been considered as an important daytime HONO source (Lee et al., 2016); (4)
108 photolysis of adsorbed nitric acid (HNO₃) and nitrate (NO₃⁻) (Ye et al., 2016; Ye et al., 2017; Zhou et al., 2002;
109 Zhou et al., 2003; Zhou et al., 2011; Ziemba et al., 2010); (5) VOC-mediated conversion of HNO₃ into HONO



110 (Gall et al., 2016).

111 Since the first atmospheric HONO measurement by Nash (1974) and the first use of long path differential UV
112 absorption technique (LP-DOAS) to measure atmospheric HONO (Perner and Platt, 1979), various measurement
113 techniques for HONO have been developed, such as spectroscopic techniques, wet chemistry-based techniques,
114 and chemical ionization mass spectrometry (CIMS). Besides DOAS technique, other spectroscopic techniques such
115 as the cavity ring-down spectroscopy (Rairoux et al., 2002), the incoherent broadband cavity-enhanced absorption
116 spectroscopy (IBBCEAS) (Gherman et al., 2008), and the cavity-enhanced absorption spectrometer (CEAS)
117 (Scharko et al., 2017) were applied in the HONO measurements. Wet chemistry techniques have the advantages of
118 higher sensitivity and lower detection limit, including long path absorption photometer (LOPAP) (Heland et al.,
119 2001; Kleffmann et al., 2003; Kleffmann et al., 2005; Kleffmann et al., 2006; Kleffmann and Wiesen, 2008; Vecera
120 and Dasgupta, 1991), AIM-IC analysis system and wet-rotating-denuder (WRD) method (Makkonen et al., 2012).
121 Very recently, CIMS techniques have been developed for fast on-line HONO measurements (Bernard et al., 2016;
122 Pinto et al., 2014; Ren et al., 2010).

123 Yangtze River Delta (YRD) region is the largest industrial zone in China and is experiencing ever increasing
124 air pollution events, characterized with high ozone (O_3) and fine particulate matters ($PM_{2.5}$) concentrations (Ding
125 et al., 2013). Despite of the great efforts in reducing sulfur dioxide (SO_2) and NO_x emissions from industrial
126 activities, high level of NO_x along with ammonia/amines have been observed near an industrial park (Zheng et al.,
127 2015b). In addition, high levels of HCHO have been frequently observed near industrial zones in China (Ma et al.,
128 2016; Wang et al., 2015b), providing an extra radical source. HONO concentrations calculated using a
129 photostationary state (PSS) approach that included homogeneous sources were found much less HONO than the
130 measured values during daytime (Kleffmann et al., 2005; Michoud et al., 2014). Lee et al. (2016) conducted a
131 detailed analysis of HONO budget and proposed that the missing daytime HONO source was related to NO_2 and
132 sunlight. A four-season measurement campaign was carried out in an urban site of Beijing and the results showed



133 monthly averaged HONO concentrations between 1.05 and 2.27 ppbv with pronounced seasonal profile (Wang et
134 al., 2017). In a recent study, Nie et al. (2015) revealed the influence of biomass burning on HONO formation at a
135 suburban site of Nanjing and demonstrated that the contribution of heterogeneous conversion of NO₂ to HONO
136 formation. However, so far, no comprehensive study on the oxidizing capability, i.e., the major contributors of OH
137 radicals, has ever been conducted in the industrial zone of YRD region.

138 In this work, we have performed HONO measurements using a custom-built wet chemistry-based method at
139 an industrial site in December 2015 in Nanjing, China. In addition, HCHO, O₃, photolysis frequencies, and other
140 trace gases and meteorological parameters were also measured. The contributions of HONO along with other OH
141 sources to OH budget were investigated using a box model based on Master Chemical Mechanism (MCM). The
142 mechanisms of possible daytime HONO formation and the consequent impacts on air pollutants formation were
143 explored.

144

145 **2 Experimental and Model Description**

146 **2.1 HONO Measurement**

147 The field measurements were carried out from 1 to 31 December 2015 on the campus of Nanjing University
148 of Information Science and Technology (NUIST) in Nanjing, China. More details about the observation site have
149 been provided in our previous work (Ma et al., 2016; Zheng et al., 2015b). Briefly, the site is located to the west of
150 clusters of steel mills and petrochemical refinery facilities and is about 15 km to the north of the downtown Nanjing.
151 All instruments were placed inside an air-conditioned trailer. In this study, a custom-built wet chemistry-based
152 HONO instrument was utilized for HONO measurements, which was originally developed by Ren et al. (2010).
153 Figure 1 is the schematics of the HONO instrument, consisting of two sample collection glass coils connected



154 successively, a 10-port injection valve (Valco Instruments Co. Inc.), a 1-m long liquid waveguide capillary cell
155 (LWCC, World Precision Instruments), and a mini spectrometer (Ocean optics, USB4000).

156 To minimize the sampling artifacts, the sampling coils were set up about 3.5 m above the ground (1.5 m above
157 the trailer rooftop) and no inlet was used. Ambient air was pulled through the coils by a vacuum pump at 1 L min⁻¹,
158 which was controlled by a mass flow controller (MKS, model M100B). In the first coil, HONO along with some
159 interfering species in the air sample were separated from the gas phase and transformed into nitrite solution by a
160 1.0 mmol L⁻¹ phosphate buffer scrubbing solution. Potential interfering species (e.g., NO₂) would also interact with
161 scrubbing solution in the second coil in a similar way as in the first coil. The nitrite solutions from the two coils
162 were then respectively mixed with sulfanilamide/N-(1-naphthyl) ethylene-diamine (SA/NED) reagents in Teflon
163 derivatization tubing and nitrite was converted via the two reactions (SR1 and SR2, see the SI for details) (Huang
164 et al., 2002). The aqueous sample was injected into the LWCC and the produced azo dye was quantified by its
165 absorption at 560 nm with a mini USB spectrometer. The difference between the absorbance signals of the two
166 coils was treated as the actual HONO signal. The HONO mixing ratio in ambient air was calculated using Eq. (1):

167
$$[\text{HONO}]_{\text{pptv}} = \frac{C_1 F_l R T}{F_g P} \times 10^{12} \quad (1)$$

168 where, C_1 is nitrite concentration (mol L⁻¹) in the scrubbing solution, F_l is the liquid flow rate (mL min⁻¹) of the
169 scrubbing solution, F_g is the sampling air flow rate (L min⁻¹), R is the ideal gas constant (8.314 m³ Pa K⁻¹mol⁻¹),
170 and T and P are the ambient temperature (294 K) and atmospheric pressure (101325 Pa), respectively, under which
171 the mass flow controller (MFC) that was used to control the sample flow rate was calibrated (Ren et al., 2010). The
172 HONO instrument was calibrated every four days using sodium nitrite standard solutions. According to the
173 calibration curve, HONO mixing ratio in ambient air can be quantified. The detection limit of the HONO instrument
174 was about 3 pptv with a time resolution of 2 min. The measurement accuracy was about ±15% at a 95% confidence
175 level (Ren et al., 2010).



176 2.2 Other measurements

177 As the observation site was part of a national standard meteorology observatory facility, meteorology
178 parameters, including wind direction, wind speed, ambient temperature, pressure and RH were continuously
179 measured. Trace gases, CO (Thermo Scientific, Model 48i), O₃ (Thermo Scientific, Model 49i), SO₂ (Thermo
180 Scientific, Model 43i) and NO_x (Thermo Scientific, Model 17i) were also measured at the observation site. The
181 Thermo Scientific 17i is designed as an ammonia (NH₃) analyzer. It basically consists of a typical NO_x analyzer
182 and an external high temperature (700°C) NH₃ converter, which is disabled and bypassed in this work. Therefore,
183 it was used as a typical NO_x analyzer. It is well known that a NO-NO_x analyzer with a molybdenum-based converter
184 can convert portion of NO_z (=NO_y-NO_x) to NO, which can then be detected as NO₂ causing an interference in NO₂
185 measurement (Villena et al., 2012). However, an aircraft study conducted in the eastern US in the winter 2015
186 found that within 6 hours of transport time, NO_x account for more than 90% of NO_y in an urban outflow (Salmon
187 et al., 2018). A sensitivity analysis showed that by decreasing the NO₂ level of 10% (an upper limit assuming all
188 NO_z were converted into NO with an efficiency of 100%), the modeled HONO decreased only by 5.3%, indicating
189 that the possible small interference in NO₂ measurement did not impact significantly on the modeled HONO results.
190 The details about the operation and calibrations of these instruments were described in previous work (Zheng et al.,
191 2015b). PM_{2.5} was observed by an online PM_{2.5} measuring instrument (METONE, BAM-1020) with a time
192 resolution of 1 hour. Aerosol surface area density was calculated using data from an WPS (wide particle
193 spectrometer, MSP model 1000XP) with a time resolution of 5 min. HCHO was measured with the DNPH method
194 from 19 to 30 December 2015 and the sampling time was 2 hours during the campaign. Detailed operation
195 procedures about the DNPH method in this study can refer to our previous work (Ma et al., 2016). Photolysis
196 frequencies (J values), including J(O¹D), J(NO₂), J(HONO), J(H₂O₂), J(HCHO), and J(NO₃), were calculated based
197 on measurements by an ultra-fast charged coupled device (CCD) detector spectrometer (Meteorology Consult
198 Gmbh, Germany). The acquisition time for J values was 1 min. Other photolysis frequencies (such as carbonyls



199 with more than two carbons) used in the model were calculated by Eq. (2) (Jenkin et al., 1997):

$$200 \quad J_i = L_i \cos(\chi) M_i \exp(-N_i \sec(\chi)) \quad (2)$$

201 where χ is the solar zenith angle; L_i , M_i , and N_i are photolysis parameters and are taken from (Jenkin et al., 1997),
202 for clear sky conditions. The calculated photolysis frequencies were then scaled by the measured $J(\text{NO}_2)$ for
203 cloudiness correction.

204 Volatile organic compounds (VOC) measurements were conducted using a commercial gas chromatograph
205 equipped with a flame ionization detector (AMA, GC5000). Sixty VOC species including C_2 - C_{12} hydrocarbons
206 were detected with a time resolution of 1 hr. Ten of the most reactive alkenes were used in the ozonolysis reaction
207 in the box model simulations.

208 **2.3 Box Model**

209 To evaluate the effect of HONO on daytime atmospheric oxidation capacity, a chemical box model with the
210 Master Chemical Mechanism (MCMv3.2) (Jenkin et al., 2012) was applied to calculate the concentrations of OH,
211 HO_2 radicals and their production and loss rates using the FACSIMILE software package (UES Software Inc.).
212 Kinetic rate coefficients were taken from the MCM website (<http://mcm.leeds.ac.uk/MCM/>). In this study, the
213 model simulation was constrained with hourly averaged measurement results, including HONO, O_3 , NO, NO_2 , CO,
214 SO_2 , HCHO, VOC, as well as water vapor, temperature, pressure, and photolysis frequencies.

215 Monte Carlo sensitivity analyses were conducted to assess the model performance. In each Monte Carlo
216 simulation, the input variables of the model, including HONO, O_3 , NO, NO_2 , CO, SO_2 , HCHO, VOCs, reaction
217 rate constants, and photolysis frequencies, were independently set to vary within $\pm 10\%$ of the mean value of
218 individual variable with a normal probability distribution.

219



220 3 Results and Discussion

221 3.1 Data Overview

222 Figure 2 shows the time series of NO, NO₂, O₃, PM_{2.5}, HONO, HCHO, J(HONO), and meteorological
223 parameters, including wind direction, wind speed, temperature, and RH. During the entire campaign period, the
224 wind speed ranged from 0.1 to 8.1 m s⁻¹ with an average of 1.7 m s⁻¹. The temperature varied between -4.1 °C and
225 16.1 °C with an average of 6.1 °C; RH varied between 17 % and 96 % with an average of 68 %.

226 During the entire measurement period, the HONO mixing ratios ranged from 0.03 ppbv to 7.04 ppbv with a
227 mean value of 1.32 ± 0.92 ppbv. Table 1 lists recent HONO observations conducted in China. Our result was
228 comparable to HONO observed in Xinken (Su et al., 2008) and Beijing (Spataro et al., 2013; Wang et al., 2017)
229 but higher than Xianghe, Beijing (Hendrick et al., 2014), Jinan (Wang et al., 2015a), Hong Kong (Xu et al., 2015)
230 and Shanghai (Wang et al., 2013). Clearly, the general trend of HONO was closely following that of NO₂, which is
231 the dominant precursor of HONO. More markedly, building up of HONO frequently proceeded the accumulations
232 of PM_{2.5}, e.g., on the 7th and from the 21st - 22nd of December 2015, indicating that HONO may promote the
233 formation of secondary aerosol by contributing to OH production, which will be further analyzed in details in the
234 following sections. The campaign averaged diurnal variations of HONO, NO₂, HONO/NO₂ ratio and aerosol S/V
235 are showed in Fig. 3. HONO started to accumulate after sunset and reached its daily maxima of ~2.0 ppbv at 08:00
236 local time (LT). Later the day, the HONO mixing ratio decreased rapidly due to its fast photolysis and increase of
237 the planetary boundary layer (PBL) height. Evidently, daytime HONO was sustained at a relatively high level. The
238 minimum of ~0.6 ppbv was observed around 16:00 LT. The mixing ratio of NO₂ varied from 9.5 ppbv to 48.7 ppbv
239 with an average of 23.9 ± 7.5 ppbv and a maximum of 27.7 ± 8.8 ppbv. NO, O₃ and PM_{2.5} mixing ratios were in
240 the range of 2.7 ppbv - 124.9 ppbv, 3 ppbv - 39 ppbv and 15 μg m⁻³ - 345 μg m⁻³, respectively. Meanwhile, the
241 HONO-to-NO₂ ratios ranged from 0.02 to 0.07, with an average of 0.05 ± 0.03 . The observed similarity between



242 the diurnal profile of HONO/NO₂ ratio and that of HONO suggested that HONO was likely originated from NO₂
243 heterogeneous reactions.

244 3.2 OH Simulation

245 Although atmosphere oxidation capacity is determined by the levels of all major oxidants in the atmosphere
246 (e.g., OH, O₃, and NO₃), OH radical is the primary oxidant in the atmosphere and series of reactions initiated by
247 OH radical can lead to the formation of other major secondary oxidants, such as O₃ and NO₃. Fully understanding
248 the budget of OH radical especially the sources of OH radical is of paramount importance for the purpose of
249 controlling the atmosphere oxidation capacity and hence to establish effective air pollution mitigation strategies.

250 *In-situ* measurement of OH radical is often limited by the availability of suitable measurement techniques,
251 which are often suffered from large amount of unresolved uncertainties (Tanner and Eisele, 1995) and the
252 observation often disagree with the modeling results to a large extent. Nevertheless, theoretically some critical
253 parameters to govern the OH radical budget in the atmosphere are difficult to measure directly, such as the
254 formation rates of OH. Accordingly, a box model is often utilized to simulate these highly reactive species to
255 investigate their photochemistry.

256 In order to assess the relative contributions of potential OH sources in this study, we have utilized a box model
257 based on the Master Chemical Mechanism (MCMv3.2) (Jenkin et al., 2012) to simulate the OH concentration and
258 the OH formation rates from various sources. The model simulation was constrained by the measurement results,
259 including HONO, O₃, NO, NO₂, CO, SO₂, VOCs, as well as water vapor, temperature, pressure, and photolysis
260 frequencies. Since HCHO measurement was only available from 19 to 30 December, simulated HCHO was used
261 for the entire campaign period. We found that the ratio between simulated to measured HCHO was 1.4 with a
262 correlation coefficient of $R^2 = 0.6$. Therefore, we applied a factor of 1.4 to the simulated HCHO in the model to
263 better represent the HCHO concentration in the atmosphere.



264 The simulated OH time series during the campaign period is shown in Fig. 4. Because the simulation is
265 constrained by the observations, only within periods when all data are available simulation were conducted.
266 Simulated OH concentration was in the range of 1.06×10^6 molecules cm^{-3} - 5.26×10^6 molecules cm^{-3} , similar to the
267 concentration observed in London (Emmerson et al., 2007), but lower than that measured in New York City (3×10^6 -
268 3.3×10^7) (Ren et al., 2003) and Guangzhou (1.5×10^7 - 2.6×10^7) (Lu et al., 2012).

269 It should be noted that the absolute values of the simulated OH may differ from the actual ambient
270 concentration. However, the general trend of OH evidently followed the solar radiation intensity, indicating its
271 photochemical production origin. Clearly, the diurnal variation of OH profile is more complicated than that of
272 photolysis rates because OH production can be affected not only by photochemical processes, but also by both
273 primary emissions (e.g., HONO and HCHO) and other non-photochemical related heterogeneous processes, such as
274 HONO production on various surfaces and ozonolysis of alkenes. These processes will be further discussed in the
275 following sections.

276 3.3 OH Formation Rates

$$277 \quad P_{OH}(HONO)_{net} = J(HONO)[HONO] - k_{OH+NO}[NO][OH] \quad (3)$$

$$278 \quad P_{OH}(O_3) = 2J(O^1D)[O_3]\phi_{OH} \quad (4)$$

$$279 \quad P_{OH}(HCHO) = 2J(HCHO)[HCHO] \quad (5)$$

$$280 \quad P_{OH}(H_2O_2) = 2J(H_2O_2)[H_2O_2] \quad (6)$$

$$281 \quad P_{OH}(O_3 + \text{alkenes}) = \sum k_{alkene(i)+O_3}[alkene(i)][OH]Y_{OH,i} \quad (7)$$

282 Previous field studies have demonstrated that HONO photolysis can contribute substantially to the OH
283 production during daytime (Elshorbany et al., 2009; Hendrick et al., 2014; Kleffmann et al., 2005; Su et al., 2008).
284 In this study, we evaluated the OH formation rates from the photolysis of HONO (Eq. 3), ozone (Eq. 4),
285 formaldehyde (Eq. 5) and hydrogen peroxide (H_2O_2) (Eq. 6), as well as ozonolysis of alkenes (Eq. 7). The second



286 term in Eq. 3 is to account for the loss of OH due to the HONO formation from OH + NO, where the OH
287 concentration was simulated using the box model, so that the net OH formation from the photolysis of HONO is
288 considered. J values are the photolysis frequencies of the corresponding species and ϕ_{OH} is the fraction of O(¹D)
289 reacts with H₂O instead of being quenched by nitrogen (N₂) or oxygen (O₂). The OH production by the photolysis
290 of formaldehyde was calculated assuming that HO₂ formed from reaction R4 was immediately converted into OH
291 by reaction R8 due to high NO levels in this polluted environment. In Eq. 7, Y_{OH_i} is the yield of OH from gas-
292 phase reaction of O₃ and alkene(i) and $k_{alkene(i)+O_3}$ is the reaction rate constant for the reaction of O₃ with alkene(i).
293 The rate constants of the ozonolysis reactions and the corresponding OH yields used in this work are listed in Table
294 2. Since H₂O₂ was not measured during this campaign, H₂O₂ was estimated from literature values, i.e., 0.5 ppbv -
295 5 ppbv (Guo et al., 2014; Hua et al., 2008; Ren et al., 2009) and a constant of 3 ppbv H₂O₂ was used in this work.

296 The calculated campaign averaged OH production rates from the photolysis of HONO, O₃, HCHO and H₂O₂
297 along with ozonolysis of alkenes were 7.13×10^6 molecules cm⁻³ s⁻¹, 2.46×10^6 molecules cm⁻³ s⁻¹, 1.60×10^6
298 molecules cm⁻³ s⁻¹, 2.39×10^5 molecules cm⁻³ s⁻¹ and 3.94×10^6 molecules cm⁻³ s⁻¹, respectively, which were
299 comparable with the literature values (Alicke et al., 2002; Chan et al., 2017; Su et al., 2008). As shown in Fig. 5.
300 the contribution of HONO photolysis to OH production varied from 23.6% to 63.3% with a mean value of 44.8%.
301 The ozonolysis of ten highly reactive alkenes (listed in Table 2) by ozone was the second largest contributor to OH
302 radical and the contribution varied from 16.1% to 60.9% with a mean of 30.3%. The contribution of ozone
303 photolysis was in the range of 1.3% to 24.7% with a mean of 14.9%. The contribution of HCHO photolysis varied
304 between 0.9% and 12.5% with a mean of 8.1%, and the contribution of H₂O₂ photolysis was negligible with an
305 average contribution of 1.9%. The contributions from different OH sources in this study was similar to those found
306 in two wintertime studies. In a study conducted in New York City in winter 2004, it was found that 48% of the net
307 HO_x production was from the HONO photolysis, 36% from the ozonolysis of alkenes, only 6% from the HCHO
308 photolysis, and 1% from the O₃ photolysis (Ren et al., 2006). In another study conducted in London in winter 2000,



309 62% of the OH production was found from the ozonolysis of alkenes, 35% from the HONO photolysis, only 6%
310 from the HCHO photolysis, and <1% from the O₃ photolysis (Heard et al., 2004).

311 The striking features of the Fig. 5 is that HONO photolysis and ozonolysis of alkenes contributed more than
312 70% of the OH production rate on average. In the early morning, HONO photolysis was the dominant source of
313 OH and may boost the photochemistry right after sunrise. As O₃ accumulated, alkene ozonolysis and O₃ photolysis
314 became more and more important. The higher percentage of the HONO photolysis in this study is most likely
315 because of the higher concentrations of HONO observed in the study area and its sources will be further investigated
316 in the following sections.

317 3.4 Industrial Plumes

318 Industrial emissions are responsible for a large portion of the haze formation in China. With the
319 implementations of more and more strict mitigation strategies, primary emissions have been reduced substantially
320 in China. However, the observation site was located just ~5 km from the Nanjing industry park, one of the largest
321 industrial zones in the YRD region, which is populated with various heavy industry facilities, including steel mills,
322 power generation stations, and petrochemical refineries. Despite the great effort to reduce primary industrial
323 emissions from these facilities, industrial plumes have often been detected at the site, carrying fair amounts of NH₃,
324 NO_x, SO₂, and VOCs (Ma et al., 2016; Zheng et al., 2015a). To investigate the effects of industrial emissions on
325 local and regional air quality and particularly the role of HONO on the transformation of primary emissions into
326 secondary air pollutants, we have paid special attention into the air masses originated from the industrial zone.
327 Figure 6 depicts the contribution fractions of OH production rates from HONO photolysis, alkene ozonolysis, O₃
328 photolysis, HCHO photolysis, and H₂O₂ photolysis during two industrial plume events. The wind rose plots in Fig.
329 6 indicate that the origin of these air masses were all from the nearby industry zone. Unlike that depicted in Fig. 5,
330 during the two industry pollution events HONO photolysis along with ozonolysis of alkenes dominated the OH



331 production throughout the day. This was most likely due to the high concentrations of NO_x and VOC within the
332 industrial plumes. More interestingly, the average $\text{PM}_{2.5}$ concentrations during the two events were 139 and 239 μg
333 m^{-3} , respectively. Evidently, HONO photolysis and ozonolysis may even play a more important role in OH
334 production during severe haze events. Although ambient OH concentrations during these events may not be high
335 (see Fig. 4a), the high levels of HONO can boost active photochemical oxidation and thus promote the formation
336 of $\text{PM}_{2.5}$, which in turn provides additional reaction surface for more HONO production. To further test this
337 hypothesis, we have investigated the HONO budgets in much details in the next section.

338 **3.5 HONO Sources**

339 **3.5.1 Primary HONO Emissions**

340 Previous studies have demonstrated that HONO can be emitted directly from vehicle exhaust (Kirchstetter et
341 al., 1996; Kurtenbach et al., 2001). To evaluate the potential impact of primary emissions on HONO concentration
342 in this work, we have calculated the contribution of primary HONO using reported HONO emission ratios, a typical
343 value of 0.8% (Kurtenbach et al., 2001) was adopted to represent the mixed Chinese vehicle fleet and accordingly
344 the fresh emitted HONO was found accounting for a maximum of 26% of the total HONO within the freshly
345 emitted plumes without consideration of dilution after they were emitted. Nevertheless, the NO/NO_x ratio measured
346 in this work was relatively low, with an average of 0.25 ± 0.06 , much less than that of freshly emitted exhausts ($>$
347 0.9) obtained from tunnel experiments (Kurtenbach et al., 2001), indicating that the air masses sampled in this work
348 had been considerably aged and mixed with other air masses, and hence primary HONO (if there was any) had
349 been diluted substantially (less than a few per cents) before reaching the observation site. In addition, our sampling
350 site is located nearby the industrial zone, and the high concentration of NO_x was mainly originated from the
351 industrial activities, so the influence of traffic source on HONO was expected to be negligible.



352 3.5.2 HONO Conversion Rate

353 The HONO conversion rate $k(\text{het})$ (hr^{-1}) is an important parameter to compare HONO formation under various
354 NO_2 levels (Xu et al., 2015). In this work, we calculate the HONO conversion rate using the Eq. (8) (Alicke et al.,
355 2003):

$$356 \quad k(\text{het}) = \frac{[\text{HONO}]_{t_2} - [\text{HONO}]_{t_1}}{(t_2 - t_1)[\text{NO}_2]} \quad (8)$$

357 where $[\text{HONO}]_{t_1}$ and $[\text{HONO}]_{t_2}$ are the HONO concentrations at two different times, t_1 and t_2 , respectively, $[\text{NO}_2]$
358 is the average NO_2 concentration between time t_1 and t_2 . Note Eq. (8) is a simplified demonstration to calculate the
359 reaction rate coefficient of the heterogeneous conversion from NO_2 to HONO at night, which can be dependent on
360 different pollution levels. In this study, the averaged $k(\text{het})$ was determined to be $\sim 0.9\% \text{ hr}^{-1}$, which was comparable
361 to the results in the urban sites of Xi'an ($0.91\% \text{ hr}^{-1}$) (Huang et al., 2017) and Shanghai ($0.7\% \text{ hr}^{-1}$), China (Wang
362 et al., 2013), but much less than some other observations, such as Back Garden, Guangdong, China ($2.4\% \text{ hr}^{-1}$) (Li
363 et al., 2012), Xinken, Guangdong, China ($1.6\% \text{ hr}^{-1}$) (Li et al., 2012) and Rossfeld, Rhine Valley, France ($2.2\% \text{ hr}^{-1}$)
364 (Acker and Möller, 2007). Nevertheless, the high level of NO_x observed in this work may still lead to high level
365 of HONO through various mechanisms.

366 3.5.3 Heterogeneous Conversion of NO_2

367 Previous studies have suggested that heterogeneous conversion of NO_2 on wet surfaces could be an important
368 nocturnal HONO source (Finlayson-Pitts et al., 2003; Wang et al., 2017). However, it appears that the proposed
369 reaction mechanism ($2\text{NO}_2 + \text{H}_2\text{O}$) was limited by the uptake of NO_2 on the wet surfaces (on the order of 10^{-6}) and
370 thus was too slow to account for the observed NO_2 to HONO conversion ratio (Kleffmann et al., 1998). Instead,
371 the reaction between NO_2 and adsorbed semi-volatile organic compounds on soot or aerosol surfaces has been
372 suggested to be one or two magnitudes faster than the aforementioned reaction (George et al., 2005; Gutzwiller et
373 al., 2002) even though the actual reaction mechanism is still under active research. Figure 7 shows the correlation



374 analyses for several individual days between HONO/NO₂ and RH, S/V, and the product of RH·S/V. For instance,
375 on 25 December 2015, HONO correlated with RH ($R^2 = 0.63$) and S/V ($R^2 = 0.70$) to some extent. However, the
376 correlations between HONO/NO₂ and the products of RH·S/V ($R^2 = 0.77$) was substantially improved, which was
377 consistent with the participation of water in heterogeneous HONO formation during nighttime, particularly on the
378 aerosol surfaces. These results were generally in line with the results of Stutz et al. (2004). It also should be noted
379 that during nighttime as ambient temperature decreased, PBL also decreased, causing the ground surface to air
380 volume ratio to increase, which may also contribute to higher NO₂ to HONO conversion efficiency (Stutz et al.,
381 2004). However, as shown in Fig. 7, HONO/NO₂ correlated with S/V to some extent and the correlation increased
382 with the product of RH and S/V. Therefore, even though the contribution of HONO formation on the ground surface
383 was present, the aerosol surface was certainly involved in the HONO formation process. The impact of RH on the
384 heterogeneous formation of HONO was further investigated. Figure 8 shows the relationship between HONO/NO₂
385 ratio and RH at night. The linearity of the bin points clearly displays the linear correlations between HONO
386 conversion ratio and RH. Following the method introduced by Stutz et al. (2004), we plotted the top-5 values of
387 HONO/NO₂ ratio (representing steady state conditions) in each 10% RH interval. The conversion efficiency of
388 NO₂ to HONO correlates very well with RH ($R^2=0.96$), strongly indicating the dependence of HONO formation
389 on RH. Similar phenomenon was also observed at an urban site (Qin et al., 2009) and a rural site (Li et al., 2012)
390 in Guangzhou, China.

391 3.5.4 Daytime HONO Budget

392 High concentrations of daytime HONO were frequently observed during the campaign period especially
393 within industrial plumes. If we assume HONO was in photostationary state involving only gas-phase homogeneous
394 HONO production and photolysis loss, the calculated daytime HONO concentration would be 8.1×10^9 molecules
395 cm⁻³, only 24.5% of the observed mean HONO concentration during daytime. Since the gas phase reaction between



396 OH and NO (i.e., P_{OH+NO}) alone was unable to explain the observed high HONO concentrations, daytime HONO
397 budget was further examined in details. Here we designate the unexplained HONO source as $P_{unknown}$. The timely
398 variation of measured HONO concentration can be expressed by the following equation (Wang et al., 2017):

$$399 \quad \frac{\partial[HONO]}{\partial t} = (P_{OH+NO} + P_{unknown}) - (L_{OH+HONO} + L_{photolysis} + L_{deposition})$$

400 (9)

401 Thus, $P_{unknown}$ can be calculated as:

$$402 \quad P_{unknown} = \frac{\partial[HONO]}{\partial t} + L_{OH+HONO} + L_{photolysis} + L_{deposition} - P_{OH+NO}$$
$$403 \quad = \frac{\partial[HONO]}{\partial t} + k_{OH+HONO}[OH][HONO] + J_{HONO}[HONO] + \frac{v_{HONO}}{H}[HONO] - k_{OH+NO}[OH][NO]$$

404 (10)

405 where $\partial[HONO]/\partial t$ represents the variation of observed HONO concentrations; $L_{photolysis}$ represents the loss rate
406 of HONO by photolysis and J_{HONO} is the measured photolysis frequency of HONO; P_{NO+OH} and $L_{OH+HONO}$ are the
407 gas-phase formation and loss rates of HONO, respectively; k_{OH+NO} and $k_{OH+HONO}$ are the corresponding reaction
408 rate constants; $L_{deposition}$ is the dry deposition rate of HONO; v_{HONO} represents deposition velocity of HONO and
409 H is the mixing height. For v_{HONO} , a value of 0.48 cm s^{-1} was adopted (Lee et al., 2016) and the observed mixing
410 height varied from 73 m to 600 m diurnally. A sensitivity analysis with and without the HONO deposition shows
411 that the modeled HONO concentration with HONO deposition loss is 3.5% lower than that without HONO
412 deposition during daytime, indicating that the dry deposition of HONO plays a minor role in HONO losses. The
413 impact of HONO direct emissions was not considered at daytime, since this term is expected to be several orders
414 of magnitude smaller than $L_{photolysis}$ (Su et al., 2008). Daytime OH concentration was not measured in this work but
415 was simulated by the MCM box model.

416 Figure 9 shows the average diurnal variation of each individual term in Eq. (10). Compared with $L_{photolysis}$, the
417 gas-phase reaction between OH and HONO and HONO dry deposition contributed very little to the HONO sink
418 during daytime. However, P_{OH+NO} and $P_{unknown}$ both contributed significantly to the HONO production and displayed



419 a completely distinct diurnal pattern. Homogeneous reaction between OH and NO reached a maximum of 1.06
420 ppbv hr⁻¹ in the early morning (09:00 LT) due to high concentrations of NO in the morning. The unknown source
421 reached a maximum of 1.46 ppbv hr⁻¹ around noontime with an average of 0.97 ppbv hr⁻¹, which was about twice
422 as much as averaged P_{OH+NO}. The diurnal profile of P_{unknown} showed a strong photo-enhanced feature, which is
423 consistent with that observed by Michoud et al. (2014) in wintertime Europe.

424 3.5.5 Photo-Enhanced Conversion of NO₂

425 The nature of the unknown source was explored by correlation analyses between P_{unknown} and other HONO
426 production related parameters (see Table 3). P_{unknown} does not correlate well with RH, NO₂, S/V, and J_{NO₂} with the
427 correlation coefficients (R²) of 0.070, 0.094, 0.107, and 0.098 respectively. The correlation increased only slightly
428 when heterogeneous conversion of NO₂ (NO₂·RH, R² = 0.161) was taken into consideration. It appeared that the
429 unknown HONO sources cannot be well explained by the heterogeneous reactions on wet surfaces alone. Previous
430 studies have suggested that light intensity could be an important parameter influencing the heterogeneous
431 conversion of NO₂ to HONO (Han et al., 2017b; Lee et al., 2016). The photo-enhanced HONO source during the
432 daytime has also been identified in different environments ranging from remote (Villena et al., 2011; Zhou et al.,
433 2002) to urban conditions (Lee et al., 2016). When photo-enhancement was also considered (J_{NO₂}·NO₂·RH, R² =
434 0.496), a significantly better correlation was achieved (Table 3). This suggests that the photosensitized reaction of
435 NO₂ on wet surfaces may be an important source of HONO during daytime. Thus, the improvement in the
436 correlation between HONO and other parameters indicates that photochemistry might indeed play an important
437 role in daytime HONO formation (George et al., 2005; Stemmler et al., 2006). Since the correlation coefficient
438 between P_{unknown} and J_{NO₂}·NO₂·RH is comparable with the value between P_{unknown} and J_{NO₂}·NO₂·S/V·RH (R² = 0.487),
439 either ground or aerosol surfaces can be the dominant reaction site for photosensitized conversion of NO₂.



440 3.5.6 Model Simulation of HONO

441 The relative contributions of potential HONO sources were assessed by a box model based on the Master
442 Chemical Mechanism (MCMv3.2) (Jenkin et al., 2012). In addition to the homogeneous reaction of NO with OH,
443 four sources of HONO were included, i.e., heterogeneous HONO formation from NO₂ reaction on aerosol surface
444 and ground surface and light-induced conversion of NO₂ on aerosols and ground surface. Dry deposition of HONO
445 was also considered and a deposition velocity of 0.48 cm s⁻¹ was used here (Lee et al., 2016).

446 Most laboratory studies suggest that the heterogeneous reaction on surface leading to HONO is proportional
447 to the first order of NO₂ (Finlayson-Pitts and Pitts, 1999), therefore the HONO formation can be represented by the
448 following reactions (Li et al., 2010):



451 where k_a and k_g are the first-order rate constants for aerosol and ground surface reactions, respectively. For the
452 heterogeneous reaction on aerosols, the first order rate constant was estimated as:

$$453 \quad k_a = \frac{\gamma_{\text{NO}_2, \text{aerosol}} \bar{v} (S/V)}{4} \quad (13)$$

454 where \bar{v} is the root mean square (RMS) velocity of NO₂, S/V is the aerosol surface area-to-volume ratio and
455 $\gamma_{\text{NO}_2, \text{aerosol}}$ is the reactive uptake coefficient on the aerosol surface, with a value of 1×10^{-6} under dark conditions
456 (Aumont et al., 2003; Li et al., 2010). Under sunlight, however, significant enhancement of NO₂ conversion to
457 HONO has been found for various types of aerosol surfaces, such as humic acid and similar organic materials
458 (Stemmler et al., 2007), soot (Monge et al., 2010), and mineral dusts (Ndour et al., 2008). To account for the
459 photoenhancement, a higher value of uptake coefficient (2×10^{-5}) was used for solar radiation less than 400 W m⁻²
460 and an uptake coefficient scaled by (light intensity)/400 for solar radiation larger than 400 W m⁻² as suggested by
461 Li et al. (2010). Accordingly, in this work the photoenhanced uptake coefficient was taken as 2×10^{-5} around the



462 morning hours (~9 AM) and was scaled by the measured photolysis rate of NO₂, i.e., (JNO₂)/ 2×10⁻³ for JNO₂ higher
463 than 2×10⁻³ (the value of JNO₂ at ~9AM).

$$464 \quad k_g = \frac{V_{d,NO_2}}{2H} \quad (14)$$

$$465 \quad V_{d,NO_2} = \frac{\gamma_{NO_2,ground} \bar{v}}{4.2} \quad (15)$$

466 Equation (14) was used to denote the heterogeneous reactions on the ground surfaces, where V_{d,NO₂} represents
467 deposition velocity of NO₂; H is the PBL height; and γ_{NO₂,ground} is the reactive uptake coefficient on the ground.
468 Here we assume an NO₂ reactive uptake coefficient of 1×10⁻⁵ (Trick, 2004) in the dark on ground surfaces with a
469 yield of 50% and increase it to 2×10⁻⁵ in the daytime, given that the photosensitized reactivity of NO₂ on the ground
470 surface is the same as on the aerosol surface. The observed boundary layer height varied from 73 m to 600 m
471 diurnally. The same scale factor ((JNO₂)/ 2×10⁻³) was also applied to the daytime ground surface reactions.

472 Figure 10a shows the averaged diurnal profiles of the measured HONO concentration and the simulated
473 HONO concentrations from different sources. In general, the box model can capture the observed HONO trend
474 with very similar magnitude of concentration, with a modeled-to-observed HONO ratio of 1.16 during the day and
475 1.40 at night. In early morning, ground surface appeared to play an important role in HONO heterogeneous
476 production while the PBL was still relatively shallow. However, after ~9:00, despite of the swift developing of PBL,
477 fine particle loading started increasing substantially (as shown in Fig. 3), indicating strong secondary formation.
478 Meanwhile, HONO production on aerosol surfaces also increased moderately. We found that higher daytime values
479 were mostly due to the light-induced conversion of NO₂ on aerosol surfaces in addition to the homogeneous reaction
480 of NO with OH. While at night, heterogeneous HONO production on ground surface dominated nocturnal HONO
481 sources and the nighttime aerosol surfaces only contributed slightly to the total nighttime HONO. The box model
482 tended to under-predict HONO during daytime, which also led to an ~1-hr delay in the peaking time of the simulated
483 HONO. The most likely reason for these disagreements is due to the fact that heterogeneous conversion of NO₂ on
484 various surfaces is too complicated to be fully represented by a single scaling parameter in a linear form.



485 Nevertheless, the general agreement between observation and simulation in this work demonstrated that photo-
486 induced NO₂ conversion on aerosol surfaces was the most important HONO source in the study area during daytime.

487 A Monte Carlo sensitivity analysis was also conducted to assess the model simulation uncertainty of HONO
488 concentration. For each of the 24 hours, 100 independent runs were performed. The Monte Carlo sensitivity
489 analysis show that the model uncertainty of HONO ranged from ±15% to ±37%. The sensitivity analysis reinforced
490 the conclusions that the proposed heterogeneous sources can generally capture the observed HONO trend.

491 To investigate the interaction between HONO chemistry and secondary aerosol formations within industrial
492 plumes, we have simulated HONO within the two industrial plume events (see Fig. 6). The results are shown in
493 Fig. 10b. Clearly, HONO was much higher within the industrial plumes comparing to the campaign average (Fig.
494 10a). In addition, aerosol surfaces were the most important HONO source during daytime (7:00 AM - 5:00 PM),
495 especially in the afternoon. Within the industrial plumes, aerosol surfaces contributed around 45% of the observed
496 daytime HONO and only about 11% of total HONO was from the ground surfaces. The fact that ground surfaces
497 were less important during daytime than nighttime was most likely due to the much higher daytime PBL, causing
498 substantial dilution of HONO formed on the ground surfaces. Meanwhile, secondary particulate matters were
499 rapidly produced within the PBL, providing additional heterogeneous reaction sites for HONO formation as a
500 strong OH source to further promote atmospheric oxidative capacity. It should be noted that the reactive uptake of
501 NO₂ on various surfaces can be highly variable with the type of surfaces. The value used here ($\sim 2 \times 10^{-5}$) is toward
502 the lower end of values reported in the literatures, which is likely the reason that the simulated HONO is generally
503 less than the observations within industrial plumes. The heterogeneous NO₂ uptake kinetics and HONO yields of
504 real atmospheric substrates are still under active study and may be different compared to the artificial surfaces
505 studied in the laboratory setting. Nevertheless, enhanced photosensitized conversion of NO₂ on aerosol surfaces is
506 demonstrated here as a major HONO source in the plumes influenced by industrial emissions.

507



508 4 Conclusions

509 Nitrous acid was measured with a custom-built wet-chemistry based HONO analyzer, together with other
510 atmospheric OH precursors (O_3 and HCHO) at a suburb site of Nanjing in December 2015. The mixing ratios of
511 HONO varied from 0.03 ppbv to 7.04 ppbv with an average of 1.32 ± 0.92 ppbv. Daytime HONO was sustained at
512 a relatively high concentration, with a minimum diurnal hourly average of ~ 0.6 ppbv observed around 16:00 LT. A
513 MCM-box model was used to investigate the HONO chemistry and its impact on atmospheric oxidation capacity
514 in the study area. The results show that the average OH production rates from the photolysis of HONO, ozonolysis
515 of alkenes, photolysis of O_3 , HCHO, and H_2O_2 were 7.13×10^6 molecules $cm^{-3} s^{-1}$, 3.94×10^6 molecules $cm^{-3} s^{-1}$,
516 2.46×10^6 molecules $cm^{-3} s^{-1}$, 1.60×10^6 molecules $cm^{-3} s^{-1}$ and 2.39×10^5 molecules $cm^{-3} s^{-1}$, respectively. The box
517 model results show that the average total OH production rate was 1.54×10^7 molecules $cm^{-3} s^{-1}$ during daytime, on
518 average about 45% from the photolysis of HONO, 30% from ozonolysis of alkenes, 15% from the photolysis of
519 O_3 , 8% from the photolysis of HCHO and 2% from the photolysis of H_2O_2 .

520 Elevated daytime HONO evidently played an important role in sustaining the atmospheric oxidative capability
521 in the study area, which cannot be explained by the typical OH+NO homogeneous formation mechanism. The
522 observed similarity between the diurnal profiles of HONO/ NO_2 ratio and HONO strongly suggests that HONO was
523 most likely originated from NO_2 heterogeneous reactions. In this study, the averaged NO_2 to HONO conversion
524 rate was determined to be $\sim 0.9\% hr^{-1}$. Good correlation between nocturnal HONO/ NO_2 and the products of S/V·RH
525 supports the heterogeneous NO_2/H_2O reaction mechanism.

526 To fully assess the HONO chemistry in the study area, an MCM box model was developed to examine HONO
527 budget. In general, the box model can capture the observed HONO trend with a modeled-to-observed HONO ratio
528 of 1.16 during the day and 1.40 at night. The model suggests that higher daytime levels of HONO were mainly
529 produced by the light-induced conversion of NO_2 on aerosol surfaces (except early morning), while the



530 heterogeneous HONO production on ground surface dominated nocturnal HONO sources. The box model tends to
531 over-predict HONO at night. The most possible reason for these discrepancies is due to the fact that heterogeneous
532 conversion of NO₂ on various surfaces was too complicated to be fully represented by a single scaling parameter
533 in a linear form. Nevertheless, the general agreement between observation and simulation in this work reiterated
534 that photo-induced NO₂ conversion on ground and aerosol surfaces was the most important HONO source in the
535 study area. In the industrial plume case study, it was demonstrated that heterogeneous photosensitized conversion
536 of NO₂ on aerosol surfaces was particularly intensified, when rapid growth of secondary particulate matters was
537 simultaneously observed. Our results indicate that the heterogeneous photosensitized conversion of NO₂ on aerosol
538 surfaces becomes the largest HONO source throughout the daytime, which in turn can enhance OH production,
539 increase the oxidative capacity of atmosphere, and further strengthen the formation of SOA during the daytime in
540 this environment.

541

542 *Author contributions*

543 JZ, YM, and XR designed the experiments, and XS, HJ, YG, WW, YZ, WZ, and YD carried out the field
544 measurements and data analysis. XS and XR performed the MCM box model simulation. JZ, XS, and YM prepared
545 the manuscript with comments from all coauthors.

546 *Acknowledgements*

547 This work was supported by the National Natural Science Foundation of China (Grant numbers 41575122,
548 41675126, and 41730106) and the National Key Research and Development Project (Grant number
549 2017YFC0209502 and 2016YFC0202401). The data used here are listed in the tables, figures, and the supporting
550 materials.

551

552 **References**



- 553 Acker, K., Möller, D., Wieprecht, W., Meixner, F. X., Bohn, B., Gilge, S., Plass-Dülmer, C., and Berresheim, H.:
554 Strong daytime production of OH from HNO₂ at a rural mountain site, *Geophys. Res. Letts.*, 33, L02809,
555 10.1029/2005GL024643, 2006.
- 556 Acker, K., and Möller, D.: Atmospheric variation of nitrous acid at different sites in Europe, *Environ. Chem.*, 4,
557 242-255, <https://doi.org/10.1071/EN07023>, 2007.
- 558 Aliche, B., Platt, U., and Stutz, J.: Impact of nitrous acid photolysis on the total hydroxyl radical budget during the
559 Limitation of Oxidant Production/Pianura Padana Produzione di Ozono study in Milan, *J. Geophys. Res. Atmos.*,
560 107, 8196, 10.1029/2000JD000075, 2002.
- 561 Aliche, B., Geyer, A., Hofzumahaus, A., Holland, F., Konrad, S., Patz, H. W., Schafer, J., Stutz, J., Volz-Thomas,
562 A., and Platt, U.: OH formation by HONO photolysis during the BERLIOZ experiment, *J. Geophys. Res. Atmos.*,
563 108, 17, 8247
564 10.1029/2001jd000579, 2003.
- 565 Ammann, M., Kalberer, M., Jost, D. T., Tobler, L., Rossler, E., Piguet, D., Gaggeler, H. W., and Baltensperger, U.:
566 Heterogeneous production of nitrous acid on soot in polluted air masses, *Nature*, 395, 157-160, 10.1038/25965,
567 1998.
- 568 Atkinson, R., and Arey, J.: Atmospheric degradation of volatile organic compounds, *Chem. Rev.*, 103, 4605-4638,
569 10.1021/cr0206420, 2003.
- 570 Aumont, B., Chervier, F., and Laval, S.: Contribution of HONO sources to the NO_x/HO_x/O₃ chemistry in the
571 polluted boundary layer, *Atmos. Environ.*, 37, 487-498, [https://doi.org/10.1016/S1352-2310\(02\)00920-2](https://doi.org/10.1016/S1352-2310(02)00920-2), 2003.
- 572 Bernard, F., Cazaunau, M., Grosselin, B., Zhou, B., Zheng, J., Liang, P., Zhang, Y., Ye, X., Daele, V., Mu, Y., Zhang,
573 R., Chen, J., and Mellouki, A.: Measurements of nitrous acid (HONO) in urban area of Shanghai, China,
574 *Environmental science and pollution research international*, 23, 5818-5829, 10.1007/s11356-015-5797-4, 2016.
- 575 Chan, K. L., Wang, S., Liu, C., Zhou, B., Wenig, M. O., and Saiz-Lopez, A.: On the summertime air quality and
576 related photochemical processes in the megacity Shanghai, China, *Sci. Total Environ.*, 580, 974-983,
577 <https://doi.org/10.1016/j.scitotenv.2016.12.052>, 2017.
- 578 Czader, B. H., Rappenglück, B., Percell, P., Byun, D. W., Ngan, F., and Kim, S.: Modeling nitrous acid and its
579 impact on ozone and hydroxyl radical during the Texas Air Quality Study 2006, *Atmos. Chem. Phys.*, 12, 6939-
580 6951, 10.5194/acp-12-6939-2012, 2012.
- 581 Ding, A. J., Fu, C. B., Yang, X. Q., Sun, J. N., Zheng, L. F., Xie, Y. N., Herrmann, E., Nie, W., Petäjä, T., Kerminen,
582 V. M., and Kulmala, M.: Ozone and fine particle in the western Yangtze River Delta: an overview of 1 yr data at
583 the SORPES station, *Atmos. Chem. Phys.*, 13, 5813-5830, 10.5194/acp-13-5813-2013, 2013.
- 584 Elshorbany, Y. F., Kurtenbach, R., Wiesen, P., Lissi, E., Rubio, M., Villena, G., Gramsch, E., Rickard, A. R., Pilling,
585 M. J., and Kleffmann, J.: Oxidation capacity of the city air of Santiago, Chile, *Atmos. Chem. Phys.*, 9, 2257-2273,
586 10.5194/acp-9-2257-2009, 2009.
- 587 Elshorbany, Y. F., Kleffmann, J., Kurtenbach, R., Lissi, E., Rubio, M., Villena, G., Gramsch, E., Rickard, A. R.,
588 Pilling, M. J., and Wiesen, P.: Seasonal dependence of the oxidation capacity of the city of Santiago de Chile,
589 *Atmos. Environ.*, 44, 5383-5394, 10.1016/j.atmosenv.2009.08.036, 2010.



- 590 Elshorbany, Y. F., Steil, B., Brühl, C., and Lelieveld, J.: Impact of HONO on global atmospheric chemistry
591 calculated with an empirical parameterization in the EMAC model, *Atmos. Chem. Phys.*, 12, 9977-10000,
592 10.5194/acp-12-9977-2012, 2012.
- 593 Emmerson, K. M., Carslaw, N., Carslaw, D. C., Lee, J. D., McFiggans, G., Bloss, W. J., Gravestock, T., Heard, D.
594 E., Hopkins, J., Ingham, T., Pilling, M. J., Smith, S. C., Jacob, M., and Monks, P. S.: Free radical modelling studies
595 during the UK TORCH Campaign in Summer 2003, *Atmos. Chem. Phys.*, 7, 167–181, doi:10.5194/acp-7-167-
596 2007, 2007.
- 597 Finlayson-Pitts, B. J., and Pitts, J. N.: *Chemistry of the upper and lower atmosphere : theory, experiments and*
598 *applications*, Academic Press, San Diego, Calif., xxii, 969 pp., 1999.
- 599 Finlayson-Pitts, B. J., Wingen, L. M., Sumner, A. L., Syomin, D., and Ramazan, K. A.: The heterogeneous
600 hydrolysis of NO₂ in laboratory systems and in outdoor and indoor atmospheres: An integrated mechanism, *PCCP*,
601 5, 223-242, 10.1039/b208564j, 2003.
- 602 Gall, E. T., Griffin, R. J., Steiner, A. L., Dibb, J., Scheuer, E., Gong, L., Rutter, A. P., Cevik, B. K., Kim, S., Lefer,
603 B., and Flynn, J.: Evaluation of nitrous acid sources and sinks in urban outflow, *Atmos. Environ.*, 127, 272-282,
604 10.1016/j.atmosenv.2015.12.044, 2016.
- 605 George, C., Strekowski, R. S., Kleffmann, J., Stemmler, K., and Ammann, M.: Photoenhanced uptake of gaseous
606 NO₂ on solid organic compounds: a photochemical source of HONO?, *Faraday Discuss.*, 130, 195-210,
607 10.1039/B417888M, 2005.
- 608 Gerecke, A., Thielmann, A., Gutzwiller, L., and Rossi, M. J.: The chemical kinetics of HONO formation resulting
609 from heterogeneous interaction of NO₂ with flame soot, *Geophys. Res. Letts.*, 25, 2453-2456, 10.1029/98GL01796,
610 1998.
- 611 Gherman, T., Venables, D. S., Vaughan, S., Orphal, J., and Ruth, A. A.: Incoherent Broadband Cavity-Enhanced
612 Absorption Spectroscopy in the near-Ultraviolet: Application to HONO and NO₂, *Environ. Sci. Technol.*, 42, 890-
613 895, 10.1021/es0716913, 2008.
- 614 Guo, J., Tilgner, A., Yeung, C., Wang, Z., Louie, P. K. K., Luk, C. W. Y., Xu, Z., Yuan, C., Gao, Y., Poon, S.,
615 Herrmann, H., Lee, S., Lam, K. S., and Wang, T.: Atmospheric Peroxides in a Polluted Subtropical Environment:
616 Seasonal Variation, Sources and Sinks, and Importance of Heterogeneous Processes, *Environ. Sci. Technol.*, 48,
617 1443-1450, 10.1021/es403229x, 2014.
- 618 Gutzwiller, L., Arens, F., Baltensperger, U., Gäggeler, H. W., and Ammann, M.: Significance of Semivolatile Diesel
619 Exhaust Organics for Secondary HONO Formation, *Environ. Sci. Technol.*, 36, 677-682, 10.1021/es015673b, 2002.
- 620 Han, C., Liu, Y., and He, H.: Heterogeneous reaction of NO₂ with soot at different relative humidity., *Environmental*
621 *Science and Pollution Research*, 24, 21248–21255, 10.1007/s11356-017-9766-y, 2017a.
- 622 Han, C., Yang, W., Yang, H., and Xue, X.: Enhanced photochemical conversion of NO₂ to HONO on humic acids
623 in the presence of benzophenone, *Environ. Pollut.*, 231, 979-986, <https://doi.org/10.1016/j.envpol.2017.08.107>,
624 2017b.
- 625 Heard, D. E., Carpenter, L. J., Creasey, D. J., Hopkins, J. R., Lee, J. D., Lewis, A. C., Pilling, M. J., Seakins, P. W.,
626 Carslaw, N., and Emmerson, K. M.: High levels of the hydroxyl radical in the winter urban troposphere, *Geophys.*



- 627 Res. Letts., 31, 10.1029/2004gl020544, 2004.
- 628 Heland, J., Kleffmann, J., Kurtenbach, R., and Wiesen, P.: A New Instrument To Measure Gaseous Nitrous Acid
629 (HONO) in the Atmosphere, *Environ. Sci. Technol.*, 35, 3207-3212, 10.1021/es000303t, 2001.
- 630 Hendrick, F., Müller, J. F., Clémer, K., Wang, P., De Mazière, M., Fayt, C., Gielen, C., Hermans, C., Ma, J. Z.,
631 Pinardi, G., Stavrakou, T., Vlemmix, T., and Van Roozendaal, M.: Four years of ground-based MAX-DOAS
632 observations of HONO and NO₂ in the Beijing area, *Atmos. Chem. Phys.*, 14, 765-781, 10.5194/acp-14-765-2014,
633 2014.
- 634 Hofzumahaus, A., Rohrer, F., Lu, K., Bohn, B., Brauers, T., Chang, C. C., Fuchs, H., Holland, F., Kita, K., Kondo,
635 Y., Li, X., Lou, S., Shao, M., Zeng, L., Wahner, A., and Zhang, Y.: Amplified trace gas removal in the troposphere,
636 *Science*, 324, 1702-1704, 10.1126/science.1164566, 2009.
- 637 Hua, W., Chen, Z. M., Jie, C. Y., Kondo, Y., Hofzumahaus, A., Takegawa, N., Chang, C. C., Lu, K. D., Miyazaki,
638 Y., Kita, K., Wang, H. L., Zhang, Y. H., and Hu, M.: Atmospheric hydrogen peroxide and organic hydroperoxides
639 during PRIDE-PRD'06, China: their concentration, formation mechanism and contribution to secondary aerosols,
640 *Atmos. Chem. Phys.*, 8, 6755-6773, 10.5194/acp-8-6755-2008, 2008.
- 641 Huang, G., Zhou, X., Deng, G., Qiao, H., and Civerolo, K.: Measurements of atmospheric nitrous acid and nitric
642 acid, *Atmos. Environ.*, 36, 2225-2235, [https://doi.org/10.1016/S1352-2310\(02\)00170-X](https://doi.org/10.1016/S1352-2310(02)00170-X), 2002.
- 643 Huang, R.-J., Yang, L., Cao, J., Wang, Q., Tie, X., Ho, K.-F., Shen, Z., Zhang, R., Li, G., Zhu, C., Zhang, N., Dai,
644 W., Zhou, J., Liu, S., Chen, Y., Chen, J., and O'Dowd, C. D.: Concentration and sources of atmospheric nitrous acid
645 (HONO) at an urban site in Western China, *Sci. Total Environ.*, 593-594, 165-172,
646 <https://doi.org/10.1016/j.scitotenv.2017.02.166>, 2017.
- 647 Jenkin, M. E., Saunders, S. M., and Pilling, M. J.: The tropospheric degradation of volatile organic compounds: a
648 protocol for mechanism development, *Atmos. Environ.*, 31, 81-104, [http://dx.doi.org/10.1016/S1352-](http://dx.doi.org/10.1016/S1352-2310(96)00105-7)
649 [2310\(96\)00105-7](http://dx.doi.org/10.1016/S1352-2310(96)00105-7), 1997.
- 650 Jenkin, M. E., Wyche, K. P., Evans, C. J., Carr, T., Monks, P. S., Alfarra, M. R., Barley, M. H., McFiggans, G. B.,
651 Young, J. C., and Rickard, A. R.: Development and chamber evaluation of the MCM v3.2 degradation scheme for
652 β -caryophyllene, *Atmos. Chem. Phys.*, 12, 5275-5308, 10.5194/acp-12-5275-2012, 2012.
- 653 Kirchstetter, T. W., Harley, A. R., and Littlejohn, D.: Measurement of nitrous acid in motor vehicle exhaust, *Environ.*
654 *Sci. Technol.*, 30, 2843-2849, 10.1021/es960135y, 1996.
- 655 Kleffmann, J., Becker, K. H., and Wiesen, P.: Heterogeneous NO₂ conversion processes on acid surfaces: possible
656 atmospheric implications, *Atmos. Environ.*, 32, 2721-2729, [https://doi.org/10.1016/S1352-2310\(98\)00065-X](https://doi.org/10.1016/S1352-2310(98)00065-X),
657 1998.
- 658 Kleffmann, J., Kurtenbach, R., Lörzer, J., Wiesen, P., Kalthoff, N., Vogel, B., and Vogel, H.: Measured and
659 simulated vertical profiles of nitrous acid-Part I: Field measurements, *Atmos. Environ.*, 37, 2949-2955,
660 10.1016/s1352-2310(03)00242-5, 2003.
- 661 Kleffmann, J., Gavriloaiei, T., Hofzumahaus, A., Holland, F., Koppmann, R., Rupp, L., Schlosser, E., Siese, M.,
662 and Wahner, A.: Daytime formation of nitrous acid: A major source of OH radicals in a forest, *Geophys. Res. Letts.*,
663 32, L05818, 10.1029/2005GL022524, 2005.



- 664 Kleffmann, J., Lörzer, J. C., Wiesen, P., Kern, C., Trick, S., Volkamer, R., Rodenas, M., and Wirtz, K.:
665 Intercomparison of the DOAS and LOPAP techniques for the detection of nitrous acid (HONO), *Atmos. Environ.*,
666 40, 3640-3652, <https://doi.org/10.1016/j.atmosenv.2006.03.027>, 2006.
- 667 Kleffmann, J., and Wiesen, P.: Technical Note: Quantification of interferences of wet chemical HONO LOPAP
668 measurements under simulated polar conditions, *Atmos. Chem. Phys.*, 8, 6813-6822, [https://doi.org/10.5194/acp-](https://doi.org/10.5194/acp-8-6813-2008)
669 [8-6813-2008](https://doi.org/10.5194/acp-8-6813-2008), 2008.
- 670 Kurtenbach, R., Becker, K. H., Gomes, J. A. G., Kleffmann, J., Lörzer, J. C., Spittler, M., Wiesen, P., Ackermann,
671 R., Geyer, A., and Platt, U.: Investigations of emissions and heterogeneous formation of HONO in a road traffic
672 tunnel, *Atmos. Environ.*, 35, 3385-3394, [https://doi.org/10.1016/S1352-2310\(01\)00138-8](https://doi.org/10.1016/S1352-2310(01)00138-8), 2001.
- 673 Lee, J. D., Whalley, L. K., Heard, D. E., Stone, D., Dunmore, R. E., Hamilton, J. F., Young, D. E., Allan, J. D.,
674 Laufs, S., and Kleffmann, J.: Detailed budget analysis of HONO in central London reveals a missing daytime
675 source, *Atmos. Chem. Phys.*, 16, 2747-2764, 10.5194/acp-16-2747-2016, 2016.
- 676 Li, G., Lei, W., Zavala, M., Volkamer, R., Dusanter, S., Stevens, P., and Molina, L. T.: Impacts of HONO sources
677 on the photochemistry in Mexico City during the MCMA-2006/MILAGO Campaign, *Atmos. Chem. Phys.*, 10,
678 6551-6567, 10.5194/acp-10-6551-2010, 2010.
- 679 Li, X., Brauers, T., Haseler, R., Bohn, B., Fuchs, H., Hofzumahaus, A., Holland, F., Lou, S., Lu, K. D., Rohrer, F.,
680 Hu, M., Zeng, L. M., Zhang, Y. H., Garland, R. M., Su, H., Nowak, A., Wiedensohler, A., Takegawa, N., Shao, M.,
681 and Wahner, A.: Exploring the atmospheric chemistry of nitrous acid (HONO) at a rural site in Southern China,
682 *Atmos. Chem. Phys.*, 12, 1497-1513, 10.5194/acp-12-1497-2012, 2012.
- 683 Liang, Y., Zha, Q., Wang, W., Cui, L., Lui, K. H., Ho, K. F., Wang, Z., Lee, S.-c., and Wang, T.: Revisiting nitrous
684 acid (HONO) emission from on-road vehicles: A tunnel study with a mixed fleet, *J. Air Waste Manage.*, 67, 797-
685 805, 10.1080/10962247.2017.1293573, 2017.
- 686 Lu, K. D., Rohrer, F., Holland, F., Fuchs, H., Bohn, B., Brauers, T., Chang, C. C., Häseler, R., Hu, M., Kita, K.,
687 Kondo, Y., Li, X., Lou, S. R., Nehr, S., Shao, M., Zeng, L. M., Wahner, A., Zhang, Y. H., and Hofzumahaus, A.:
688 Observation and modelling of OH and HO₂ concentrations in the Pearl River Delta 2006: a missing OH source in
689 a VOC rich atmosphere, *Atmos. Chem. Phys.*, 12, 1541-1569, 10.5194/acp-12-1541-2012, 2012.
- 690 Ma, Y., Diao, Y., Zhang, B., Wang, W., Ren, X., Yang, D., Wang, M., Shi, X., and Zheng, J.: Detection of
691 formaldehyde emissions from an industrial zone in the Yangtze River Delta region of China using a proton transfer
692 reaction ion-drift chemical ionization mass spectrometer, *Atmos. Meas. Tech.*, 9, 6101-6116, 10.5194/amt-9-6101-
693 2016, 2016.
- 694 Makkonen, U., Virkkula, A., Mäntykenttä, J., Hakola, H., Keronen, P., Vakkari, V., and Aalto, P. P.: Semi-
695 continuous gas and inorganic aerosol measurements at a Finnish urban site: comparisons with filters, nitrogen in
696 aerosol and gas phases, and aerosol acidity, *Atmospheric Chemistry and Physics*, 12, 5617-5631, 10.5194/acp-12-
697 5617-2012, 2012.
- 698 Michoud, V., Colomb, A., Borbon, A., Miet, K., Beekmann, M., Camredon, M., Aumont, B., Perrier, S., Zapf, P.,
699 Siour, G., Ait-Helal, W., Afif, C., Kukui, A., Furger, M., Dupont, J. C., Haefelin, M., and Doussin, J. F.: Study of
700 the unknown HONO daytime source at a European suburban site during the MEGAPOLI summer and winter field
701 campaigns, *Atmospheric Chemistry and Physics*, 14, 2805-2822, 10.5194/acp-14-2805-2014, 2014.



- 702 Monge, M. E., D'Anna, B., Mazri, L., Giroir-Fendler, A., Ammann, M., Donaldson, D. J., and George, C.: Light
703 changes the atmospheric reactivity of soot, *Proc. Natl. Acad. Sci. USA*, 107, 6605-6609, 10.1073/pnas.0908341107,
704 2010.
- 705 Müller, M., Anderson, B. E., Beyersdorf, A. J., Crawford, J. H., Diskin, G. S., Eichler, P., Fried, A., Keutsch, F. N.,
706 Mikoviny, T., Thornhill, K. L., Walega, J. G., Weinheimer, A. J., Yang, M., Yokelson, R. J., and Wisthaler, A.: In
707 situ measurements and modeling of reactive trace gases in a small biomass burning plume, *Atmos. Chem. Phys.*,
708 16, 3813-3824, 10.5194/acp-16-3813-2016, 2016.
- 709 Nakashima, Y., and Kajii, Y.: Determination of nitrous acid emission factors from a gasoline vehicle using a chassis
710 dynamometer combined with incoherent broadband cavity-enhanced absorption spectroscopy, *Sci. Total Environ.*,
711 575, 287-293, <https://doi.org/10.1016/j.scitotenv.2016.10.050>, 2017.
- 712 Nash, T.: Nitrous acid in the atmosphere and laboratory experiments on its photolysis, *Tellus*, 26, 175-179,
713 10.3402/tellusa.v26i1-2.9768, 1974.
- 714 Ndour, M., D'Anna, B., George, C., Ka, O., Balkanski, Y., Kleffmann, J., Stemmler, K., and Ammann, M.:
715 Photoenhanced uptake of NO₂ on mineral dust: Laboratory experiments and model simulations, *Geophys. Res.*
716 *Letts.*, 35, L05812, 10.1029/2007gl032006, 2008.
- 717 Neftel, A., Blatter, A., Hesterberg, R., and Staffelbach, T.: Measurements of concentration gradients of HNO₂ and
718 HNO₃ over a semi-natural ecosystem *Atmos. Environ.*, 30 (17), 3017-3025, 1996.
- 719 Neuman, J. A., Trainer, M., Brown, S. S., Min, K.-E., Nowak, J. B., Parrish, D. D., Peischl, J., Pollack, I. B.,
720 Roberts, J. M., Ryerson, T. B., and Veres, P. R.: HONO emission and production determined from airborne
721 measurements over the Southeast U.S., *J. Geophys. Res. Atmos.*, 121, 9237-9250, 10.1002/2016JD025197, 2016.
- 722 Nie, W., Ding, A. J., Xie, Y. N., Xu, Z., Mao, H., Kerminen, V. M., Zheng, L. F., Qi, X. M., Huang, X., Yang, X.
723 Q., Sun, J. N., Herrmann, E., Petaja, T., Kulmala, M., and Fu, C. B.: Influence of biomass burning plumes on
724 HONO chemistry in eastern China, *Atmos. Chem. Phys.*, 15, 1147-1159, 10.5194/acp-15-1147-2015, 2015.
- 725 Perner, D., and Platt, U.: Detection of nitrous-acid in the atmosphere by differential optical-absorption, *Geophys.*
726 *Res. Letts.*, 6, 917-920, 10.1029/GL006i012p00917, 1979.
- 727 Pinto, J. P., Dibb, J., Lee, B. H., Rappenglück, B., Wood, E. C., Levy, M., Zhang, R. Y., Lefer, B., Ren, X. R., Stutz,
728 J., Tsai, C., Ackermann, L., Golovko, J., Herndon, S. C., Oakes, M., Meng, Q. Y., Munger, J. W., Zahniser, M., and
729 Zheng, J.: Intercomparison of field measurements of nitrous acid (HONO) during the SHARP campaign, *J.*
730 *Geophys. Res. Atmos.*, 119, 5583-5601, 10.1002/2013JD020287, 2014.
- 731 Platt, U., Perner, D., Harris, G. W., Winer, A. M., and Pitts Jr, J. N.: Observations of nitrous acid in an urban
732 atmosphere by differential optical absorption, *Nature*, 285, 312, 10.1038/285312a0, 1980.
- 733 Qin, M., Xie, P., Su, H., Gu, J., Peng, F., Li, S., Zeng, L., Liu, J., Liu, W., and Zhang, Y.: An observational study of
734 the HONO-NO₂ coupling at an urban site in Guangzhou City, South China, *Atmos. Environ.*, 43, 5731-5742,
735 <https://doi.org/10.1016/j.atmosenv.2009.08.017>, 2009.
- 736 Rairoux, P., Koch, B., Moller, D., Görnitz, G., Warmbier, G., and Czyzewski, A.: Atmospheric traces monitoring
737 applying Cavity Ring-Down Spectroscopy, *Environmental Science and Pollution Research*, Special issue 4, 68-71,
738 2002.



- 739 Ren, X., Brune, W. H., Mao, J., Mitchell, M. J., Leshner, R. L., Simpas, J. B., Metcalf, A. R., Schwab, J. J., Li, Y.,
740 Demerjian, K. L., Felton, H. D., Boynton, G., Adams, A., Perry, J., He, Y., Zhou, X., and Hou, J.: Behavior of OH
741 and HO₂ in the winter atmosphere in New York City: Observations and model comparison, *Atmos. Environ.*, **40**,
742 S252–S263, 10.1016/j.atmosenv.2005.11.073, 2006.
- 743 Ren, X., Gao, H., Zhou, X., Crouse, J. D., Wennberg, P. O., Browne, E. C., LaFranchi, B. W., Cohen, R. C., McKay,
744 M., Goldstein, A. H., and Mao, J.: Measurement of atmospheric nitrous acid at Blodgett Forest during
745 BEARPEX2007, *Atmos. Chem. Phys.*, **10**, 6283–6294, 10.5194/acp-10-6283-2010, 2010.
- 746 Ren, X. R., Harder, H., Martinez, M., Leshner, R. L., Oligier, A., Simpas, J. B., Brune, W. H., Schwab, J. J., Demerjian,
747 K. L., He, Y., Zhou, X. L., and Gao, H. G.: OH and HO₂ chemistry in the urban atmosphere of New York City,
748 *Atmos. Environ.*, **37**, 3639–3651, 10.1016/s1352-2310(03)00459-x, 2003.
- 749 Ren, Y., Ding, A., Wang, T., Shen, X., Guo, J., Zhang, J., Wang, Y., Xu, P., Wang, X., and Gao, J.: Measurement of
750 gas-phase total peroxides at the summit of Mount Tai in China, *Atmospheric Environment*, **43**, 1702–1711,
751 10.1016/j.atmosenv.2008.12.020, 2009.
- 752 Rickard, A. R., Johnson, D., McGill, C. D., and Marston, G.: OH Yields in the Gas-Phase Reactions of Ozone with
753 Alkenes, *The Journal of Physical Chemistry A*, **103**, 7656–7664, 10.1021/jp9916992, 1999.
- 754 Rondon, A., and Sanhueza, E.: High HONO atmospheric concentrations during vegetation burning in the tropical
755 savannah, *Tellus B: Chemical and Physical Meteorology*, **41**, 474–477, 10.3402/tellusb.v41i4.15102, 1989.
- 756 Salmon, O. E., Shepson, P. B., Ren, X., He, H., Hall, D. L., Dickerson, R. R., Stirm, B. H., Brown, S. S., Fibiger,
757 D. L., McDuffie, E. E., Campos, T. L., Gurney, K. R., and Thornton, J. A.: Top-Down Estimates of NO_x and CO
758 Emissions From Washington, D.C.-Baltimore During the WINTER Campaign, *J. Geophys. Res. Atmos.*, **123**,
759 7705–7724, 10.1029/2018jd028539, 2018.
- 760 Scharko, N. K., Martin, E. T., Losovyj, Y., Peters, D. G., and Raff, J. D.: Evidence for Quinone Redox Chemistry
761 Mediating Daytime and Nighttime NO₂-to-HONO Conversion on Soil Surfaces, *Environ. Sci. Technol.*, **51**, 9633–
762 9643, 10.1021/acs.est.7b01363, 2017.
- 763 Sörgel, M., Trebs, I., Wu, D., and Held, A.: A comparison of measured HONO uptake and release with calculated
764 source strengths in a heterogeneous forest environment, *Atmospheric Chemistry and Physics*, **15**, 9237–9251,
765 10.5194/acp-15-9237-2015, 2015.
- 766 Spataro, F., Ianniello, A., Esposito, G., Allegrini, I., Zhu, T., and Hu, M.: Occurrence of atmospheric nitrous acid
767 in the urban area of Beijing (China), *Sci. Total Environ.*, **447**, 210–224,
768 <https://doi.org/10.1016/j.scitotenv.2012.12.065>, 2013.
- 769 Stemmler, K., Ammann, M., Donders, C., Kleffmann, J., and George, C.: Photosensitized reduction of nitrogen
770 dioxide on humic acid as a source of nitrous acid, *Nature*, **440**, 195–198, 10.1038/nature04603, 2006.
- 771 Stemmler, K., Ndour, M., Elshorbany, Y., Kleffmann, J., D'Anna, B., George, C., Bohn, B., and Ammann, M.: Light
772 induced conversion of nitrogen dioxide into nitrous acid on submicron humic acid aerosol, *Atmos. Chem. Phys.*, **7**,
773 4237–4248, 10.5194/acp-7-4237-2007, 2007.
- 774 Stutz, J., Alicke, B., Ackermann, R., Geyer, A., Wang, S. H., White, A. B., Williams, E. J., Spicer, C. W., and Fast,
775 J. D.: Relative humidity dependence of HONO chemistry in urban areas, *J. Geophys. Res. Atmos.*, **109**, D03307,



- 776 doi:10.1029/2003jd004135, 2004.
- 777 Su, H., Cheng, Y. F., Shao, M., Gao, D. F., Yu, Z. Y., Zeng, L. M., Slanina, J., Zhang, Y. H., and Wiedensohler, A.:
778 Nitrous acid (HONO) and its daytime sources at a rural site during the 2004 PRIDE-PRD experiment in China, J.
779 Geophys. Res. Atmos., 113, D14312, 10.1029/2007JD009060, 2008.
- 780 Su, H., Cheng, Y., Oswald, R., Behrendt, T., Trebs, I., Meixner, F. X., Andreae, M. O., Cheng, P., Zhang, Y., and
781 Poschl, U.: Soil nitrite as a source of atmospheric HONO and OH radicals, Science, 333, 1616-1618,
782 10.1126/science.1207687, 2011.
- 783 Tang, Y., An, J., Wang, F., Li, Y., Qu, Y., Chen, Y., and Lin, J.: Impacts of an unknown daytime HONO source on
784 the mixing ratio and budget of HONO, and hydroxyl, hydroperoxyl, and organic peroxy radicals, in the coastal
785 regions of China, Atmos. Chem. Phys., 15, 9381-9398, 10.5194/acp-15-9381-2015, 2015.
- 786 Tanner, D. J., and Eisele, F. L.: Present oh measurement limits and associated uncertainties, J. Geophys. Res. Atmos.,
787 100, 2883-2892, 1995.
- 788 Trick, S.: Formation of nitrous acid on urban surfaces - a physicalchemical perspective, Ph.D. thesis, University of
789 Heidelberg, 2004.
- 790 Trinh, H. T., Imanishi, K., Morikawa, T., Hagino, H., and Takenaka, N.: Gaseous nitrous acid (HONO) and nitrogen
791 oxides (NO_x) emission from gasoline and diesel vehicles under real-world driving test cycles, J. Air Waste Manage.,
792 67, 412-420, 10.1080/10962247.2016.1240726, 2017.
- 793 VandenBoer, T. C., Brown, S. S., Murphy, J. G., Keene, W. C., Young, C. J., Pszenny, A. A. P., Kim, S., Warneke,
794 C., de Gouw, J. A., Maben, J. R., Wagner, N. L., Riedel, T. P., Thornton, J. A., Wolfe, D. E., Dubé, W. P., Öztürk,
795 F., Brock, C. A., Grossberg, N., Lefer, B., Lerner, B., Middlebrook, A. M., and Roberts, J. M.: Understanding the
796 role of the ground surface in HONO vertical structure: High resolution vertical profiles during NACHTT-11, J.
797 Geophys. Res. Atmos., 118, 10,155-110,171, 10.1002/jgrd.50721, 2013.
- 798 Vecera, Z., and Dasgupta, P. K.: Measurement of ambient nitrous acid and a reliable calibration source for gaseous
799 nitrous acid, Environ. Sci. Technol., 25, 255-260, 10.1021/es00014a006, 1991.
- 800 Villena, G., Kleffmann, J., Kurtenbach, R., Wiesen, P., Lissi, E., Rubio, M. A., Croxatto, G., and Rappenglück, B.:
801 Vertical gradients of HONO, NO_x and O₃ in Santiago de Chile, Atmos. Environ., 45, 3867-3873,
802 10.1016/j.atmosenv.2011.01.073, 2011.
- 803 Villena, G., Bejan, I., Kurtenbach, R., Wiesen, P., and Kleffmann, J.: Interferences of commercial NO₂ instruments
804 in the urban atmosphere and in a smog chamber, Atmos. Meas. Tech., 5, 149-159, 10.5194/amt-5-149-2012, 2012.
- 805 Wall, K. J., and Harris, G. W.: Uptake of nitrogen dioxide (NO₂) on acidic aqueous humic acid (HA) solutions as a
806 missing daytime nitrous acid (HONO) surface source, J. Atmos. Chem., 74, 283-321, 10.1007/s10874-016-9342-
807 8, 2016.
- 808 Wang, J., Zhang, X., Guo, J., Wang, Z., and Zhang, M.: Observation of nitrous acid (HONO) in Beijing, China:
809 Seasonal variation, nocturnal formation and daytime budget, Sci. Total Environ., 587-588, 350-359,
810 <https://doi.org/10.1016/j.scitotenv.2017.02.159>, 2017.
- 811 Wang, L., Wen, L., Xu, C., Chen, J., Wang, X., Yang, L., Wang, W., Yang, X., Sui, X., Yao, L., and Zhang, Q.:



- 812 HONO and its potential source particulate nitrite at an urban site in North China during the cold season, *The Science*
813 of the total environment, 538, 93-101, 10.1016/j.scitotenv.2015.08.032, 2015a.
- 814 Wang, M., Chen, W. T., Shao, M., Lu, S. H., Zeng, L. M., and Hu, M.: Investigation of carbonyl compound sources
815 at a rural site in the Yangtze River Delta region of China, *Journal of Environmental Sciences-China*, 28, 128-136,
816 10.1016/j.jes.2014.12.001, 2015b.
- 817 Wang, S., Zhou, R., Zhao, H., Wang, Z., Chen, L., and Zhou, B.: Long-term observation of atmospheric nitrous
818 acid (HONO) and its implication to local NO₂ levels in Shanghai, China, *Atmos. Environ.*, 77, 718-724,
819 <https://doi.org/10.1016/j.atmosenv.2013.05.071>, 2013.
- 820 Wong, K. W., Oh, H. J., Lefer, B. L., Rappenglück, B., and Stutz, J.: Vertical profiles of nitrous acid in the nocturnal
821 urban atmosphere of Houston, TX, *Atmos. Chem. Phys.*, 11, 3595-3609, 10.5194/acp-11-3595-2011, 2011.
- 822 Wong, K. W., Tsai, C., Lefer, B., Haman, C., Grossberg, N., Brune, W. H., Ren, X., Luke, W., and Stutz, J.: Daytime
823 HONO vertical gradients during SHARP 2009 in Houston, TX, *Atmospheric Chemistry and Physics*, 12, 635-652,
824 10.5194/acp-12-635-2012, 2012.
- 825 Wong, K. W., Tsai, C., Lefer, B., Grossberg, N., and Stutz, J.: Modeling of daytime HONO vertical gradients during
826 SHARP 2009, *Atmos. Chem. Phys.*, 13, 3587-3601, 10.5194/acp-13-3587-2013, 2013.
- 827 Xu, Z., Wang, T., Wu, J., Xue, L., Chan, J., Zha, Q., Zhou, S., Louie, P. K. K., and Luk, C. W. Y.: Nitrous acid
828 (HONO) in a polluted subtropical atmosphere: Seasonal variability, direct vehicle emissions and heterogeneous
829 production at ground surface, *Atmos. Environ.*, 106, 100-109, <http://dx.doi.org/10.1016/j.atmosenv.2015.01.061>,
830 2015.
- 831 Xue, L., Gu, R., Wang, T., Wang, X., Saunders, S., Blake, D., Louie, P. K. K., Luk, C. W. Y., Simpson, I., Xu, Z.,
832 Wang, Z., Gao, Y., Lee, S., Mellouki, A., and Wang, W.: Oxidative capacity and radical chemistry in the polluted
833 atmosphere of Hong Kong and Pearl River Delta region: analysis of a severe photochemical smog episode,
834 *Atmospheric Chemistry and Physics*, 16, 9891-9903, 10.5194/acp-16-9891-2016, 2016.
- 835 Ye, C., Zhou, X., Pu, D., Stutz, J., Festa, J., Spolaor, M., Tsai, C., Cantrell, C., Mauldin, R. L., Campos, T.,
836 Weinheimer, A., Hornbrook, R. S., Apel, E. C., Guenther, A., Kaser, L., Yuan, B., Karl, T., Haggerty, J., Hall, S.,
837 Ullmann, K., Smith, J. N., Ortega, J., and Knote, C.: Rapid cycling of reactive nitrogen in the marine boundary
838 layer, *Nature*, 532, 489-491, 10.1038/nature17195, 2016.
- 839 Ye, C., Zhang, N., Gao, H., and Zhou, X.: Photolysis of Particulate Nitrate as a Source of HONO and NO_x, *Environ.*
840 *Sci. Technol.*, 51, 6849-6856, 10.1021/acs.est.7b00387, 2017.
- 841 Zhang, N., Zhou, X., Shepson, P. B., Gao, H., Alaghmand, M., and Stirm, B.: Aircraft measurement of HONO
842 vertical profiles over a forested region, *Geophys. Res. Letts.*, 36, L15820, 10.1029/2009gl038999, 2009.
- 843 Zheng, J., Ma, Y., Chen, M., Zhang, Q., Wang, L., Khalizov, A. F., Yao, L., Wang, Z., Wang, X., and Chen, L.:
844 Measurement of atmospheric amines and ammonia using the high resolution time-of-flight chemical ionization
845 mass spectrometry, *Atmos. Environ.*, 102, 249-259, <http://dx.doi.org/10.1016/j.atmosenv.2014.12.002>, 2015a.
- 846 Zheng, J., Ma, Y., Chen, M., Zhang, Q., Wang, L., Khalizov, A. F., Yao, L., Wang, Z., Wang, X., and Chen, L.:
847 Measurement of atmospheric amines and ammonia using the high resolution time-of-flight chemical ionization
848 mass spectrometry, *Atmospheric Environment*, 102, 249-259, 10.1016/j.atmosenv.2014.12.002, 2015b.



849 Zhou, X., Civerolo, K., Dai, H., Huang, G., Schwab, J., and Demerjian, K.: Summertime nitrous acid chemistry in
850 the atmospheric boundary layer at a rural site in New York State, *J. Geophys. Res. Atmos.*, 107, ACH 13-11-ACH
851 13-11, 10.1029/2001jd001539, 2002.

852 Zhou, X., Gao, H., He, Y., Huang, G., Bertman, S. B., Civerolo, K., and Schwab, J.: Nitric acid photolysis on
853 surfaces in low-NO_x environments: Significant atmospheric implications, *Geophys. Res. Letts.*, 30, 2217,
854 10.1029/2003gl018620, 2003.

855 Zhou, X., Zhang, N., TerAvest, M., Tang, D., Hou, J., Bertman, S., Alaghmand, M., Shepson, P. B., Carroll, M. A.,
856 Griffith, S., Dusanter, S., and Stevens, P. S.: Nitric acid photolysis on forest canopy surface as a source for
857 tropospheric nitrous acid, *Nature Geoscience*, 4, 440-443, 10.1038/ngeo1164, 2011.

858 Ziemba, L. D., Dibb, J. E., Griffin, R. J., Anderson, C. H., Whitlow, S. I., Lefer, B. L., Rappenglück, B., and Flynn,
859 J.: Heterogeneous conversion of nitric acid to nitrous acid on the surface of primary organic aerosol in an urban
860 atmosphere, *Atmos. Environ.*, 44, 4081-4089, 10.1016/j.atmosenv.2008.12.024, 2010.

861

862



863 **Table 1.** Overview on HONO measurements performed in Nanjing and other cities in China.

Location	Date	HONO (ppbv) [#]	References
Beijing	Sep. - Oct. 2015 (autumn)	2.27 ± 1.82	Wang et al. (2017)
	Jan. 2016 (winter)	1.05 ± 0.89	
	Apr. - May 2016 (spring)	1.05 ± 0.95	
	Jun. - Jul. 2016 (summer)	1.38 ± 0.90	
Xi'an	Jul. - Aug. 2015 (summer)	1.12 ± 0.97	Huang et al. (2017)
Jinan	Nov. 2013 - Jan. 2014 (winter)	0.35 ± 0.5	Wang et al. (2015a)
Nanjing	Apr. - Jun. 2012 (spring)	0.76 ± 0.79	Nie et al. (2015)
Xianghe	Mar 2010 - Dec 2012	0.33 ± 0.16 [*]	Hendrick et al. (2014)
Beijing	Jan. - Feb. 2007(winter)	1.04 ± 0.73	Spataro et al. (2013)
Guangzhou	Jul. 2006 (summer)	0.71~8.43 (2.8) ^{**}	Qin et al. (2009)
Xinken	Oct. - Nov. 2004 (autumn)	0.4~3.8 (1.2) ^{**}	Li et al. (2012)
Nanjing	Dec. 2015 (winter)	1.32 ± 0.92	This work

864 [#] Campaign averaged; ^{*} Yearly average; ^{**} Only range and mean values are reported

865



866 **Table 2.** Ozonolysis reaction rate constants and OH formation yields of the volatile organic compounds (VOC)

867 used in the calculation.

VOC	$k(298\text{K}) \times 10^{-18}$ ($\text{cm}^3 \text{molecule}^{-1} \text{s}^{-1}$) ^a	OH yield	VOC	$k(298\text{K}) \times 10^{-18}$ ($\text{cm}^3 \text{molecule}^{-1} \text{s}^{-1}$) ^a	OH yield
Ethene	1.6	0.13 ^b	trans-2-Pentene	160	0.47 ^c
Propene	10.1	0.34 ^b	cis-2-Pentene	130	0.3 ^c
trans-2-Butene	190	0.59 ^b	1-Pentene	10.6	0.37 ^b
cis-2-Butene	125	0.37 ^b	Isoprene	12.8 ^c	0.13 ± 0.03 ^c
1-Butene	9.64	0.41 ^b	Styrene	17	0.07 ^c

868 a: Atkinson and Arey (2003); b: Rickard et al. (1999); c: Alicke et al. (2002)

869

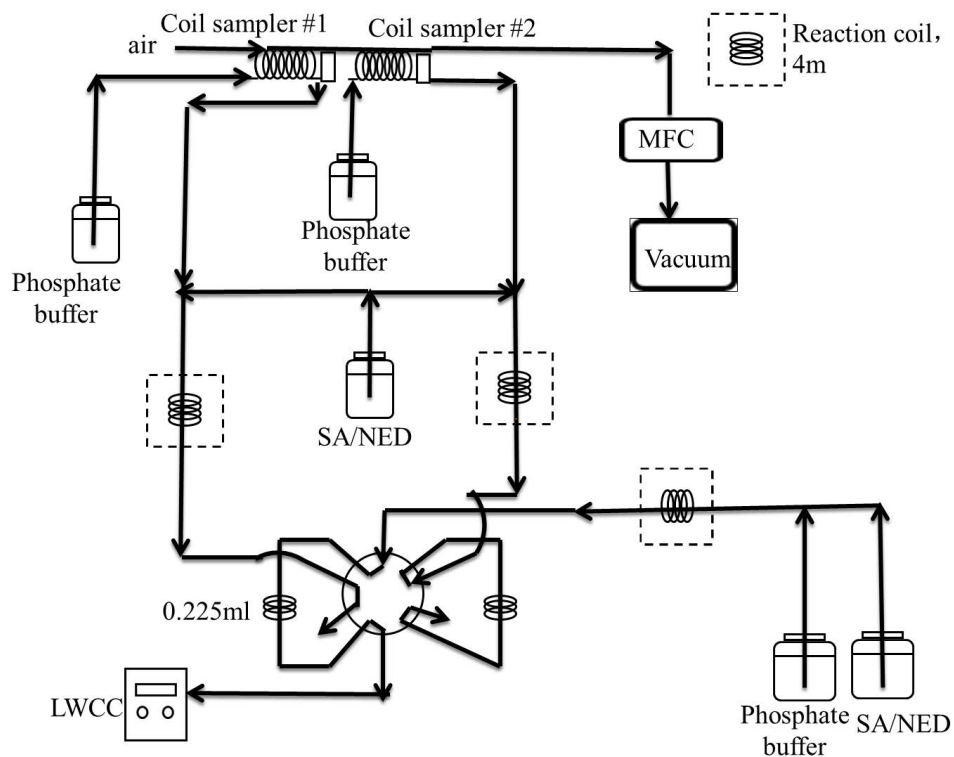


870 **Table 3.** Linear correlation coefficients (Pearson correlation, R^2) of the unknown source to HONO production-
871 related parameters.

Individual	Correlation Coefficient (R^2)	Various Combinations of	Correlation Coefficient (R^2)
RH	0.070	$J(\text{NO}_2) \cdot \text{S}/\text{V}$	0.350
NO_2	0.094	$J(\text{NO}_2) \cdot \text{NO}_2$	0.261
S/V	0.107	$J(\text{NO}_2) \cdot \text{RH}$	0.348
$J(\text{NO}_2)$	0.098	$J(\text{NO}_2) \cdot \text{NO}_2 \cdot \text{RH}$	0.496
$\text{NO}_2 \cdot \text{S}/\text{V}$	0.126	$J(\text{NO}_2) \cdot \text{NO}_2 \cdot \text{S}/\text{V}$	0.372
$\text{NO}_2 \cdot \text{RH}$	0.161	$\text{NO}_2 \cdot \text{RH} \cdot \text{S}/\text{V}$	0.191
$\text{RH} \cdot \text{S}/\text{V}$	0.149	$J(\text{NO}_2) \cdot \text{NO}_2 \cdot \text{S}/\text{V} \cdot \text{RH}$	0.487

872

873

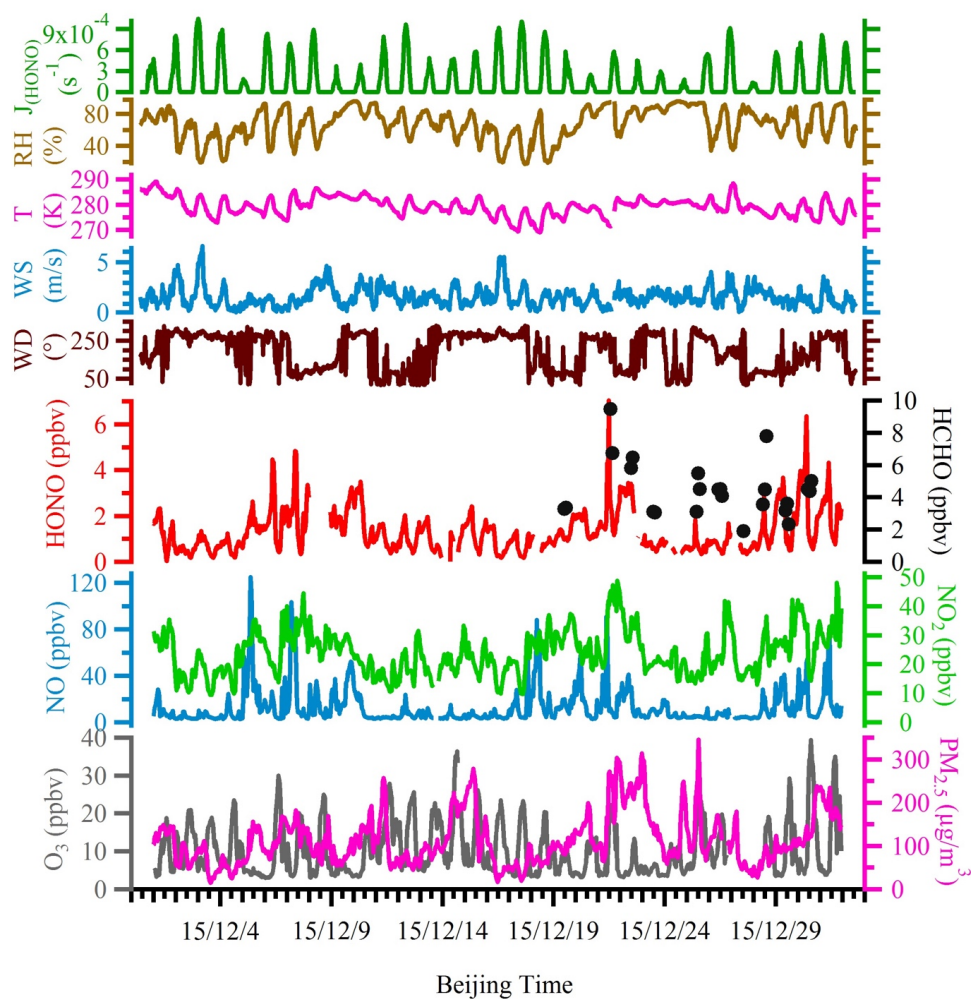


874

875

Figure 1. Schematics of the custom-built wet chemistry-based HONO instrument.

876



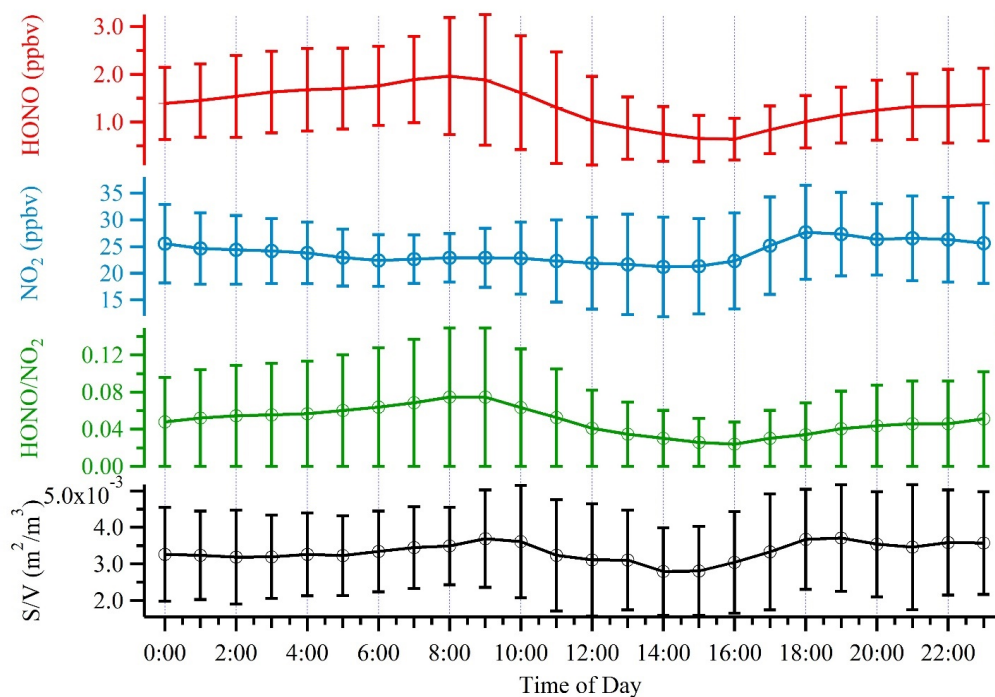
877

878 **Figure 2.** Time series of meteorological parameters, including HONO photolysis frequency ($J(\text{HONO})$), relative
879 humidity (RH), ambient temperature, wind speed and wind direction, as well as mixing ratios of measured HONO,
880 HCHO, NO, NO₂, O₃ and PM_{2.5} during the observation period.

881



882

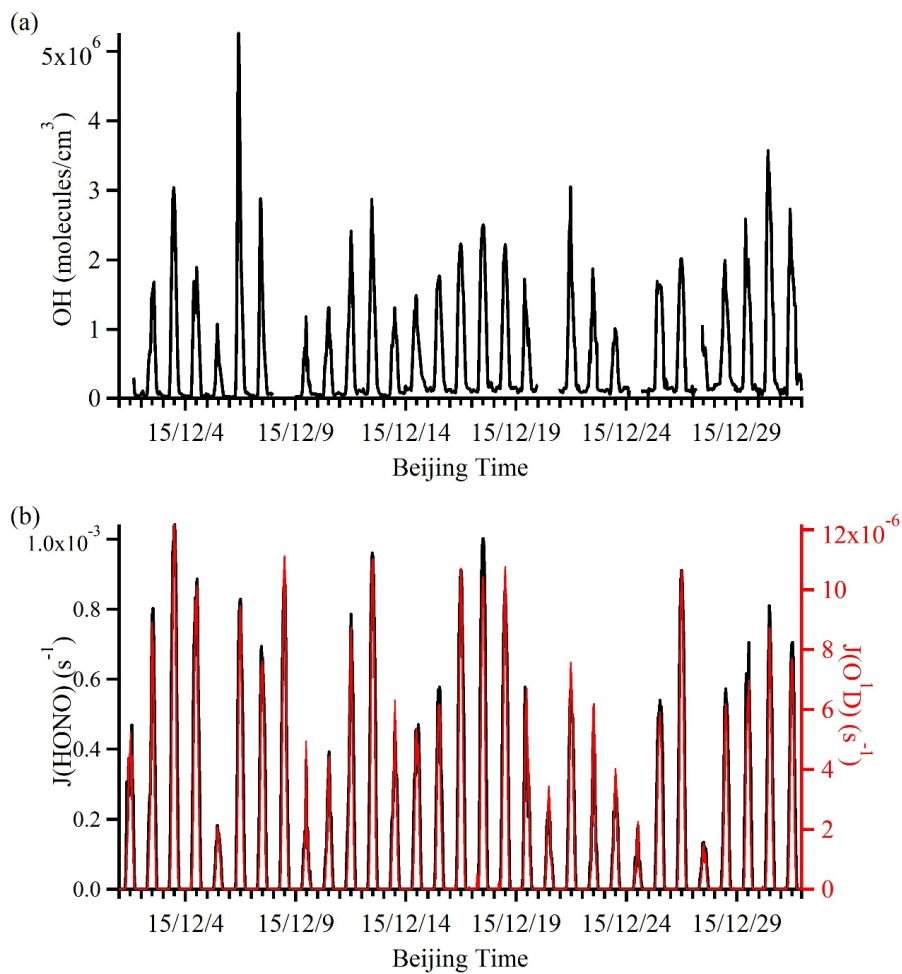


883

884 **Figure 3.** Average diurnal profiles of HONO, NO₂, HONO/NO₂ and S/V. Error bars represent the standard

885 deviations in hourly bins.

886



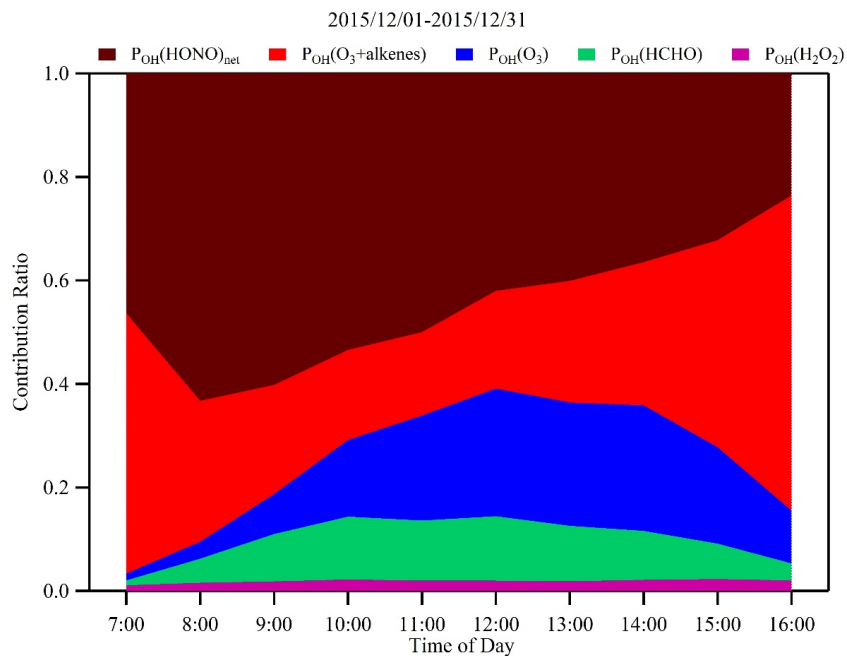
887

888

889 **Figure 4.** Time series of simulated OH (panel a) and observed photolysis rates ($J(\text{HONO})$ and $J(\text{O}^1\text{D})$) (panel b).

890 The gaps in the OH time series were the time periods when some observation data were not available.

891



892

893 **Figure 5.** Campaign averaged diurnal variations of contribution fractions of OH production rates from HONO

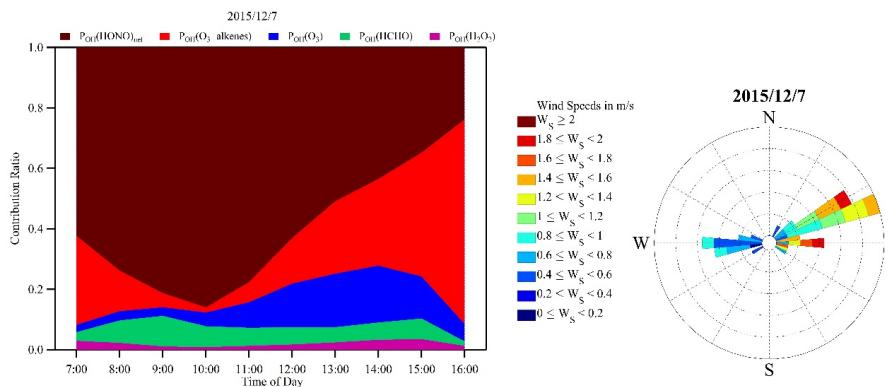
894 photolysis (brown), alkene ozonolysis (red), O_3 photolysis (blue), HCHO photolysis (green), and H_2O_2 photolysis

895 (purple).

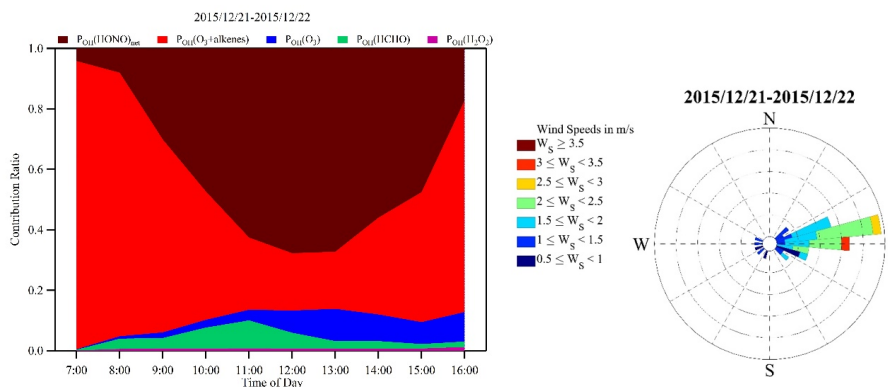
896



897



898



899

900

901 **Figure 6.** The same plots as Fig. 5 during two industrial plume events on the 7th (upper panel) and from the 21st-

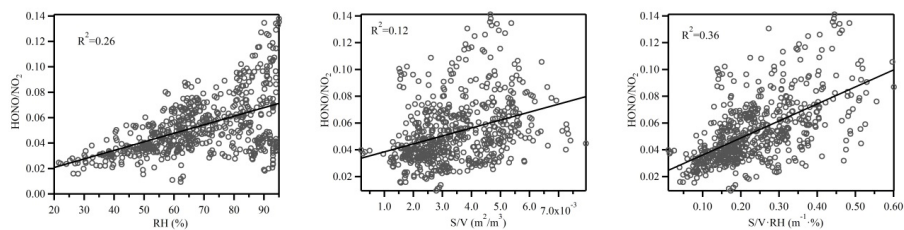
902 22nd (lower panel) of December. The corresponding rose plots indicate the origin of these plumes, i.e., the industry

903 park to the east of the observation site.

904



905

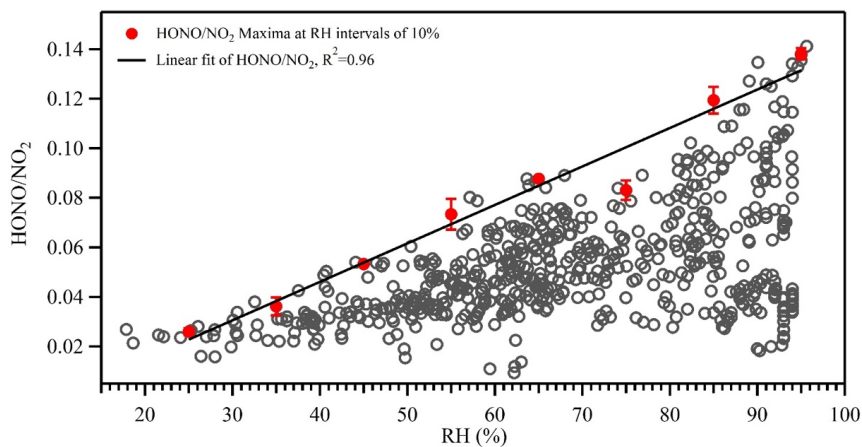


906

907

Figure 7. Nighttime correlations between HONO/NO₂ and RH, S/V and the product of S/V·RH.

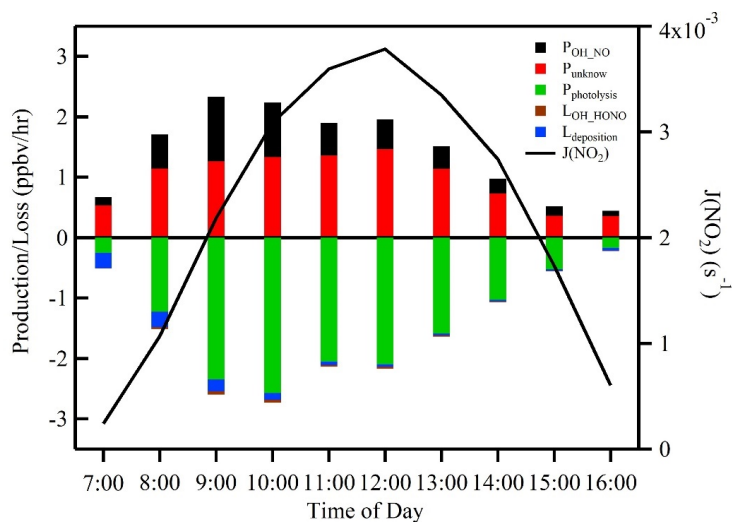
908



909

910 **Figure 8.** Correlation between HONO/NO₂ and relative humidity (RH) at night. The open gray circles are 30-min
911 averages. The red circles represent the averages of the top-5 maxima of HONO/NO₂ ratios in 10% RH bins. Error
912 bars represent standard deviations of the top-5 HONO/NO₂ ratios in 10% RH bins. The black line is linear fit of
913 the red circles for HONO/NO₂ with RH.

914

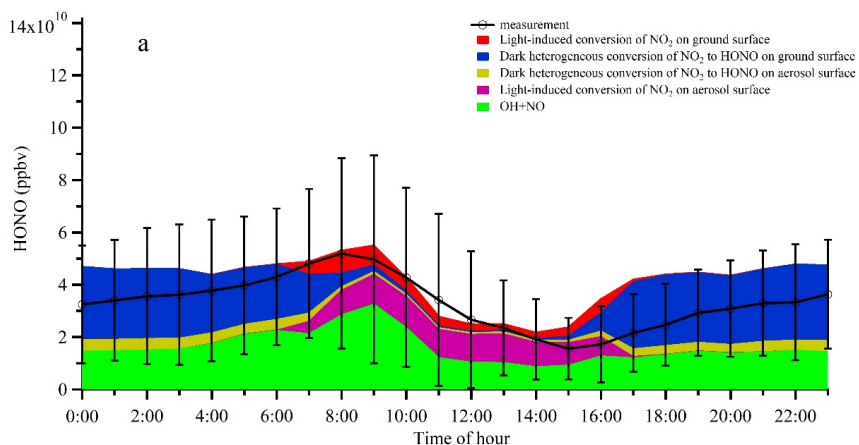


915

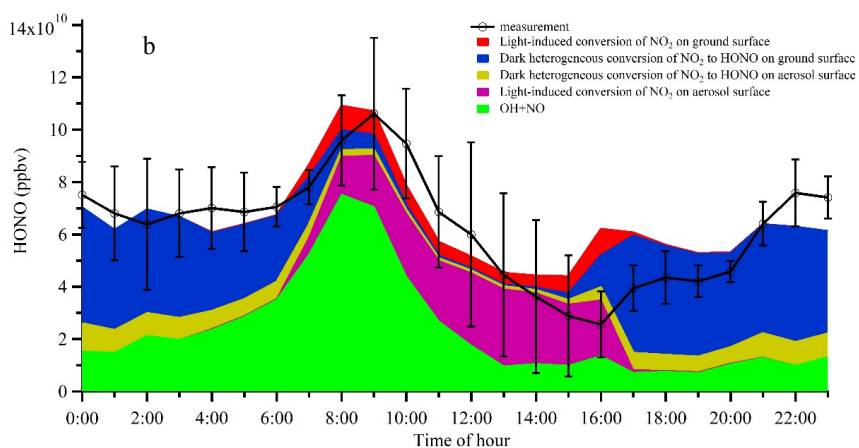
916 **Figure 9.** Averaged production and loss rates of daytime HONO and $J(NO_2)$ during the measurement period. The

917 black line shows the photolysis rate of NO_2 .

918



919



920

921 **Figure 10.** a) Averaged diurnal profiles of the measured HONO and the modeled HONO from different sources.

922 Error bars on the black line represent standard deviations of HONO measurements in hourly bins. Stacked areas

923 show contributions of different HONO sources to the modeled HONO concentration; b) The same plot as panel a,

924 except that only the two industrial plume events (the 7th and from the 21st to 22nd) were considered in the model.

925